The Kupol'noe Silver-Tin Deposit (Sakha Republic, Russia): An Example of the Evolution of an Ore-Magmatic System

Article *in* Geology of Ore Deposits · November 2001

Geology of Ore Deposits, Vol. 43, No. 6, 2001, pp. 442–467. Translated from Geologiya Rudnykh Mestorozhdenii, Vol. 43, No. 6, 2001, pp. 495–523.

The Kupol'noe Silver–Tin Deposit (Sakha Republic, Russia): an Example of the Evolution of an Ore–Magmatic System

G. N. Gamyanin*, N. S. Bortnikov, V. V. Alpatov*, E. Yu. Anikina**, A. S. Borisenko***, A. A. Borovikov***, A. G. Bakharev*, Yu. Ya. Zhdanov*, and L. P. Nosik****

**Institute of Geology of Diamond and Precious Metals, Siberian Division, Russian Academy of Sciences, pr. Lenina 39, Yakutsk, 677891 Russia*

***Institute of Geology of Ore Deposits, Petrography, Mineralogy and Geochemistry, Russian Academy of Sciences, Staromonetnyi per. 35, Moscow, 109017 Russia*

****United Institute of Geology, Geophysics, and Mineralogy, Siberian Division, Russian Academy of Sciences, pr. Koptyuga 3, Novosibirsk, 630090 Russia*

Received March 1, 2001

Abstract—A study of temporal relationships and a formation sequence of tin, silver–base metal, and silver–antimony ores; chemical compositions of minerals; fluid inclusions, and stable isotope (S, O, and C) ratios in minerals from the Kupol'noe silver–tin deposit was carried out. The deposit is confined to the Sarychev ring volcano–plutonic structure in the southeast of the Verkhoyansk–Kolyma orogenic belt. It occurs in granodiorites, the Rb–Sr age of which is 125 Ma, and around this granite massif in a hornfel zone. Ore bodies are mineralized cataclastic zones and carbonate–quartz veins with sulfides that are accompanied by greisen, quartz–carbonate–sericite, and argillized rocks. Principal minerals are quartz, carbonates, galena, pyrite, and sphalerite; subordinate minerals are cassiterite, stannite, tetrahedrite, arsenopyrite, and silver–antimony sulfosalts. The deposit was formed as a result of multiply repeated hydrothermal activity. Three types of ore mineralization have been recorded: rare metal (tin–tungsten), tin–silver–base metal, and silver–antimony. The fluid inclusion study showed that the rare metal mineralization was formed from heterogenized fluids with a high chloride content (36–38 wt %) at 250 to 450°C . Major productive carbonate–polysulfide and silver–antimony mineral associations were deposited from low-temperature solutions (125–250°C) with a salinity of 3.3 to 9.2 wt % NaCl-equiv. The $\delta^{18}O$ values of quartz I, quartz II, quartz III, and quartz IV are +6.2 to +7.9‰, +7.1 to +8.9‰, +2.3 to +5.5‰, and +8.3 to +11.0‰, respectively. The $\delta^{18}O$ and $\delta^{13}C$ values of carbonates vary from +17.4 to +29.2‰ and –15.0 to –5.6‰, respectively. The $\delta^{34}S$ of sulfides range from –4.2 to +6.0‰. Calculated ratios of oxygen isotopes in water suggest that ore-forming fluids evolved from a fluid with a predominantly magmatic component in which heated meteoric water played a substantial role. A hypothesis on the overprinting of mineralizations deposited in mesothermal and epithermal environments at different stages of geodynamic history of this region is suggested.

INTRODUCTION

Numerous silver–base metal deposits are known in the accretionary–fold belts in the Northeast of Russia which underwent a complicated geodynamic history as a result of a collision of a superterrane with a craton. This collision led to the formation of the batholithic belts. An intense growth of the continent occurred at accretion of terranes due to intermittent movement of the subduction zones towards the ocean (Parfenov, 1995). A tectonomagmatic activation of fold belts related to the formation of Okhotsk–Chukotka volcano–plutonic belt played an important role in metallogeny of these structures. Thereof, a spatial superposition of the different mineralization types occurs in many ore districts and fields in the Northeast of Russia. It was shown that data on chemical and isotopic composition of fluids can lead to an understanding of the origin of deposits and relationship of ore-forming processes with different development megastages of this region (Bortnikov *et al.*, 1998; Gamyanin *et al.*, 1998).

The Kupol'noe silver–tin deposit is situated on the eastern slope of the Sarychev Range, in the basin of the Eimyu River, a left tribute of the Nera River, 130 km southeast from the Ust'-Nera settlement. Three different types of ore mineralization are telescoped on its area: tin, silver–base metal, and silver–antimony. Researches of the mineral deposits in the Verkhoyansk–Kolyma mesozoids have held different viewpoints on genetic links between these mineralization types. During the geological prospecting in the Verkhne–Taryn region, Sukhoverkov (written communication, 1980) distinguished ores of two types: gold–silver ores genetically related to subvolcanic dacites, and tin–base metal ores associated with Early Cretaceous granitoids. Flerov (1976) recorded quartz–cassiterite and galena–sphalerite types among cassiterite–sulfide deposits. Naiborodin *et al.* (1974) considered these deposits as a specific genetic style. Nekrasova and Demin (1977) suggested a facial transition of one ore type to another and isolated these deposits as a specific volcanogenic

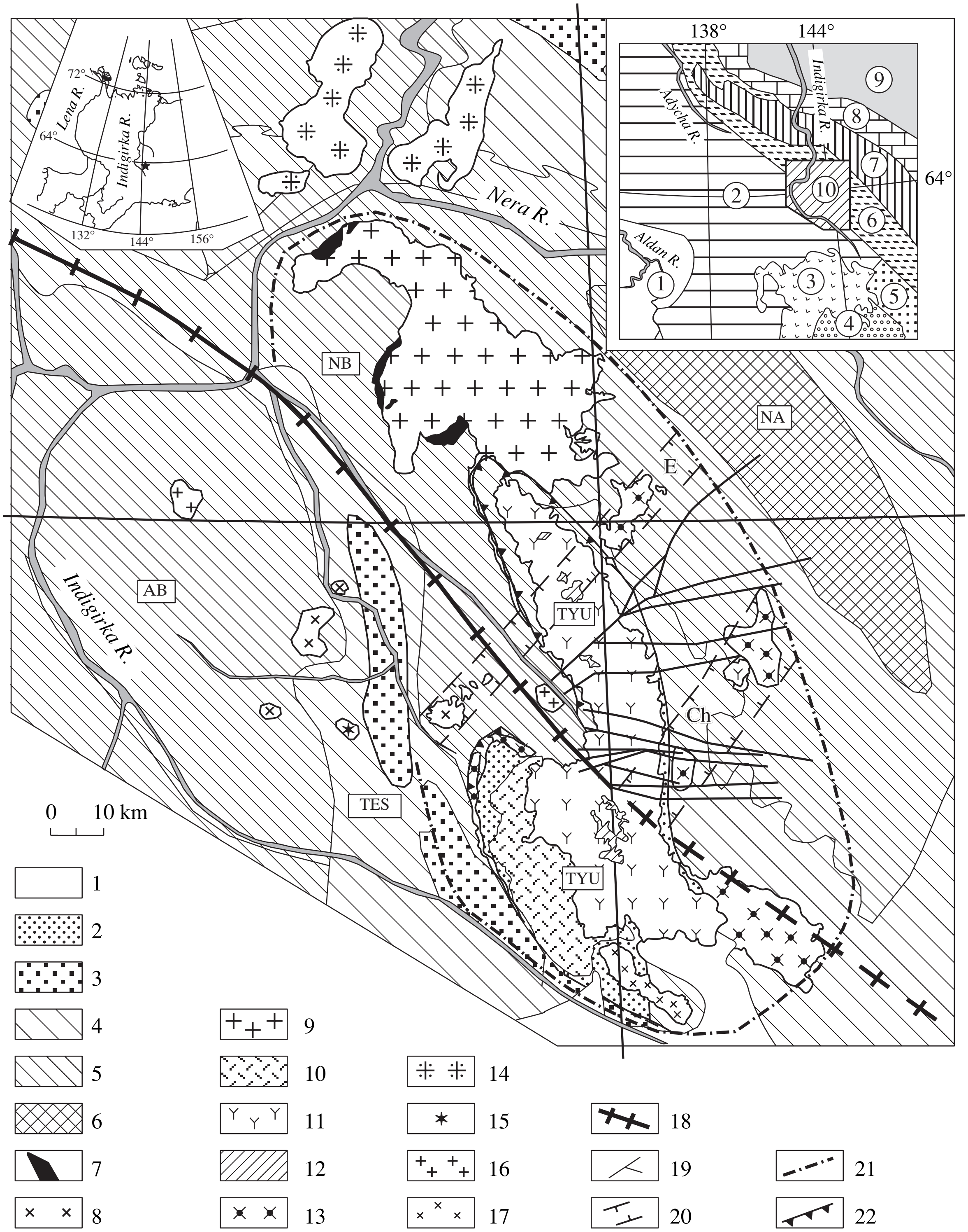

Fig. 1. Tectonic scheme of the Sarychev volcano–plutonic ring structure. (1) Quaternary formation; (2) upper Cretaceous volcanogenic–sedimentary deposits; (3)–(6) terrigenous rocks: 3—Early and Middle Jurassic, 4—Norian, 5—Karnian stage of upper Triassic, 6—middle and low Triassic; (7)–(17) magmatic complexes: 7—Late Jurassic diorite, 8–10—Early Neocomian: 8—granodiorite–granite, 9—adamellite-granite, 10—rhyolite, 11–13—Late Neocomian: 11—dacite, 12—dacite with micropegmatite granodiorite-porphyry, 13—granodiorite, 14—Aptian–Albian granite–leucogranite, 15—Albian granodiorite, 16—Cenomanian adamellite, 17—Turonian–Early Cenomanian granodiorite-porphyry; (18) Adycha–Taryn fault zone; (19) faults; (20) fault zones; (21) Sarychev ring (after Rudich); (22) zones of arc faults and fold structures: NA—Nerskii anticlinorium, AB—Adycha brachyanticline, TES—Taryn–El'ginsk synclinorium, NB—Nelkansk brachyanticline, TYU—Taryn–Yuryakhsk graben-syncline; fault zones: E—Ergelyakhsk, Ch—Chingansk. On insert (number in cycles): 1—Siberian Platform, 2—Verkhoyansk fold belt, 3—Okhotsk–Chukotka belt, 4—Okhotsk craton, 5—Velichinsk terrane, 6—Kular–Nersk terrane, 7—In'yali–Debinsk fore arc trough, 8—Uyandino–Yasachninsk volcanic arc, 9—Ilin'–Tasskii anticlinorium, 10—study area.

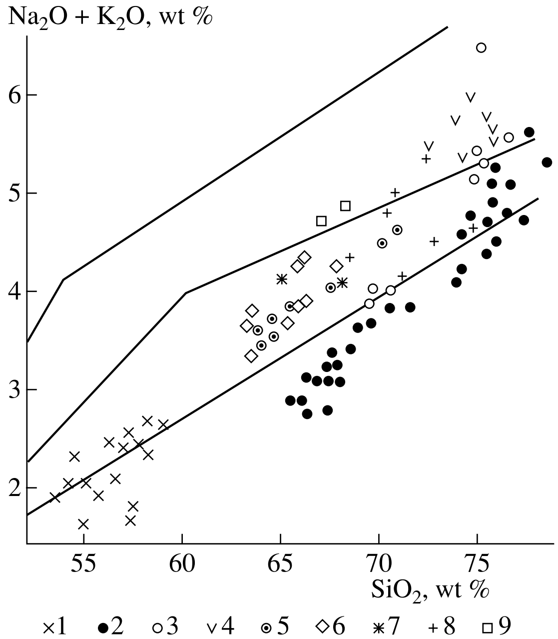

Fig. 2. K_2O vs. SiO_2 plot from magmatic rocks of Late Jurassic diorite (1); Early Neocomian: granodiorite–granite (2); adamellite–granite (3); rhyolite (4); Late Neocomian dacite (5); Aptian granodiorite (6); Albian granodiorite (7); Cenomanian adamellite (8); Early Cenomanian granodiorite-porphyry (9) complexes.

gold–silver type. Kosovets *et al.* (1984) assumed that the hybrid tin–silver–antimony deposits were formed at the intersection of two regional structures: the Adycha–Taryn fault zone controlling gold–silver mineralization, and a submeridional transregional lineament hosting the silver mineralization.

These conclusions were mainly based on results of geological and mineralogical studies. There were no data on the composition of mineral-forming fluids and the ratio of stable isotopes in minerals from these deposits. This did not lead to a conclusion on the origin and sources of fluids and their constituents. The temporal relationships of the different mineralization styles and mineral compositions of metasomatic wall rocks and ores and their chemical composition were poorly characterized. To elucidate genetic links between tin, silver–base metal, and silver–antimony ores and fluid sources, the authors studied temporal relationships and the formation sequence of these ores, the chemical compositions of minerals, and the fluid inclusions and stable isotope (S, O, and C) ratios in minerals. These data were used to determine the composition and sources of a mineral-forming fluid(s) and conditions and mechanisms of the mineral deposition.

GEOLOGICAL STRUCTURE OF THE DISTRICT AND DEPOSIT

Regional Geology

The Kupol'noe deposit is localized in a central part of the large (7500 km^2) Sarychev ring volcano–plutonic structure in the southeastern Verkhoyansk–Kolyma orogenic belt (Fig. 1). This volcano–plutonic structure intersects the Adycha–Taryn fault system and unites the Verkhoyansk fold–thrust belt and the Kular–Nera terrane (Parfenov, 1995).

The Taryn massif of subvolcanic dacites is situated in the center of the Sarychev ring structure. The ^{40}Ar-^{39}Ar age of these rocks is 134 to 138 Ma (Layer *et al.*, 2001). Early to Middle Jurassic terrigenous rocks outcrop as an intermittent band of 1 to 10 km wide around the subvolcanic massif. Thin (2–3 m) interlayers of subalkaline basalts, lagoon–continental sediments with ash-flow siliceous tuff interbeds, and continental rhyolite and their tuffs are found among terrigenous rocks. These sequences dip gently and compose 110-km-long and 20- to 40-km-wide limbs of the Taryn–Yuryakhsk graben-syncline extending north–northwest to the Sarychev Ridge. The graben-syncline forms an inner ring of the Sarychev volcano–plutonic structure. Its outer ring is 10–20 km wide and is formed by a series of granitoid intrusions belonging to the Late Jurassic to Early Cretaceous, Early Cretaceous, and Late Cretaceous complexes (Bakharev *et al.*, 1997).

Granitoids of the Nel'kansk massif, composed of biotite adamellite and granodiorite, are referred to the Late Jurassic–Early Cretaceous complex. The ^{40}Ar-^{39}Ar dating of biotite of these rocks showed that they were injected 139.8 to 144.8 Ma ago at the collision of the Kolyma–Omolon superterrane with the Verkhoyansk passive margin (Layer *et al.*, 2001; Nedosekin and Shkodzinskii, 1991).

The Early Cretaceous complex includes granitoids of the Arga–Salinsk, Chingakansk, Odonkansk, Trud, and Kapriznyi massifs localized to the east of the Sarychev ring structure. Rocks of this complex are younger than dacites of the Taryn subvolcano (Rudich, 1959; Popov and Kuznetsov, 1987). The chemical compositions of rocks of the complex and the Taryn subvolcano correspond to that of the S-type granitoids, but display features of I- and transitional IS-granites. On the SiO_2–($Na_2O + K_2O$) plot, compositional points of granitoids of major phases of the granodiorite massifs and dacites of the Taryn subvolcano form a general trend of normal alkalinity (Fig. 2). These rocks are peraluminous (ASI = 1.1 to 1.6) and are richer in normative corundum (0.64–7.7 wt %). The Rb–Sr dating of biotite and feldspars has shown that the isotopic age of the Trud and Odonkan quartz diorite and granodiorite massifs is 125–124 Ma. Their emplacement corresponded to the Early Cretaceous magmatic epoch in the Kolyma–Okhotsk region. Rocks of these complexes are considered to have been formed during a late orogenic development megastage of the region (Kotlyar *et al.*, 2000).

Similar chemical compositions of the Early Cretaceous granodiorite complex and dacites of the Taryn subvolcano indicate their comagmatic character. Geophysical studies found these rocks to be derivates of a deep-seated intermediate magma chamber. Inside the

Sarychev volcano–plutonic ring structure, the Taryn gravity minimum has been found (Stognii *et al.*, 1999, 2000). Deep structure modeling of the Sarychev structure has shown that this anomaly can be explained by a blind granite–gneiss dome.

Granitoids of the Baryllyekhsk and Kuranakh–Salinsk massifs are included in the Late Cretaceous complex. The first one is composed of adamellite, while the second one consists of granodiorite-porphyry. The injection of these rocks as shown by Rb–Sr and ^{40}Ar-^{39}Ar dating of bulk samples and biotite occurred 86 to 96 Ma ago. Their formation was related to the development of the Chukotka–Okhotsk volcano–plutonic belt (Layer *et al.*, 2001).

Four fault systems of submeridional, northwestern, northeastern, and sublatitudinal strikes are distinguished in the area of the Sarychev ring structure.

Steeply dipping to the west submeridional, faults are traced along the eastern limb of the Taryn–Yuryakhsk graben-syncline. They are marked by positive magnetic anomalies extending as a linear zone 27 km long and 5 km wide. These faults are considered to be abyssal and relatively more ancient structures. They control the distribution of dikes and stocks of Early to Middle Jurassic subalkaline gabbro–diabases and dolerites.

The Adycha–Taryn fault zone is referred to the northwestern fault system. Thrust and slip displacements, predominantly left-slip movements, occurred along these faults (Parfenov *et al.*, 1988). It branches into a system of sublatitudinal faults within the Taryn subvolcano.

The Ergelyakhsk and Chingakansk fault zones that control the Late Jurassic–Late Cretaceous granitoid intrusions and intersect the Taryn subvolcano belong to the northeastern system. They extend along strike for 70 and 40 km and are 8 and 15 km wide, respectively.

Geology of the Deposit

The Kupol'noe deposit, occupying an area of 4×8 km, is localized in the outer ring of the eastern part of the Sarychev structure. It is hosted by granitoids of the Trud and Kapriznyi massifs and hornfelses surrounding these massifs (Fig. 3). The deposit and massifs are situated on the western limb of the Eimyunsk brachyanticline of the Nersk anticlinorium conjugated with the Taryn–Yuryakhsk graben-syncline in the west. The brachyanticline extends in the north–northwestern direction for 20–25 km and is about 15 km wide. Early and Late Norian terrigenous rocks are exposed in the core of this fold, while Late Norian siltstones and mudstones compose its limbs. The basal cement of these rocks contains abundant carbonaceous matter. The western limb of the Eimyunsk brachyanticline is complicated with linear and brachyform folds up to 1.5 km wide and a northeastern orientation.

The Trud and Kapriznyi massifs, that have areas of 12 km^2 and 6 km^2, respectively, display rather irregular contacts in aerial view. In watersheds of the Trud and Kapriznyi creeks, the massifs are separated by a narrow (less than 1.5 km) zone of sedimentary rocks that underwent contact metamorphism. Possibly, these massifs are the outcrops of a single intrusive body elongated in the submeridional direction.

The Trud and Kapriznyi massifs consist of Middle- and Late Jurassic diorite complex and Early Cretaceous granodiorite complex. The first one includes diorites and quartz diorites that constitute 3.5% of the total area of these massifs. Diorites occur as xenoblocks (0.1–0.2 km^2) within granodiorites in the southern part of the Trud massif and an endocontact zone of the Kapriznyi massif. The ^{40}Ar-^{39}Ar dating of biotite from these rocks has shown their age to be between 161.8 ± 0.8 Ma and 152.1 ± 0.8 Ma (Layer *et al.*, 2001). The granodiorite complex is represented by granodiorites, adamellites, aplitelike granites, aplites, as well as granodiorite-porphyry dikes.

Granodiorites occupy about 80% of the total area of the massif's outcrops. Ortho- and clinopyroxene are present in association with plagioclase, orthoclase, and biotite, the principal minerals of these rocks. Common accessory minerals are ilmenite, apatite, zircon, and garnet. Three varieties of garnet were recognized. They are substantially different due to variation of a pyrope component content (25–28, 19, and 13–15 mol %) and ferrugenity (71–74, 80, and 85–87 mol %). The occurrence of two varieties of garnet suggests that parent magma was generated in the gneiss–granulite layer of the Pre-Riphean basement (Ermolov *et al.*, 1979). A typical feature of granodiorites is the presence of graphite segregations, which contains up to 10 vol % in some places. Granodiorites are characterized by a definite geochemical specialization. The Sn, Pb, and Sb concentrations that are the major ore constituents in the deposit are 1.5–2 times higher than their clarke content in silicic rocks.

Granodiorite-porphyries compose two thick (100–120 m wide) and short (less than 900 m long) dikes in the northeastern exocontact zone of the Trud massif. The dikes dip at angles of 60 to 70° toward the massif, and cut it. Granodiorite-porphyries are different from granodiorites of the major phase due to higher Al_2O_3, Na_2O, and CaO contents and a lower F amount. They are richer in alkaline (7.05–8.10 wt %), while K prevails over Na. Aluminiferous and agpaitic coefficients of granite-porphyries and granodiorites are identical. In contrast to the latter, higher Pb, Zn, Sr, Mo, As, and Sb contents were detected in granodiorite-porphyries, while the Sn and Ag concentrations are lower. The contents of these elements are higher relative to the clarke values. The age of the granodiorite-porphyry dikes determined by the K–Ar technique is 100 Ma (Nenashev, 1979).

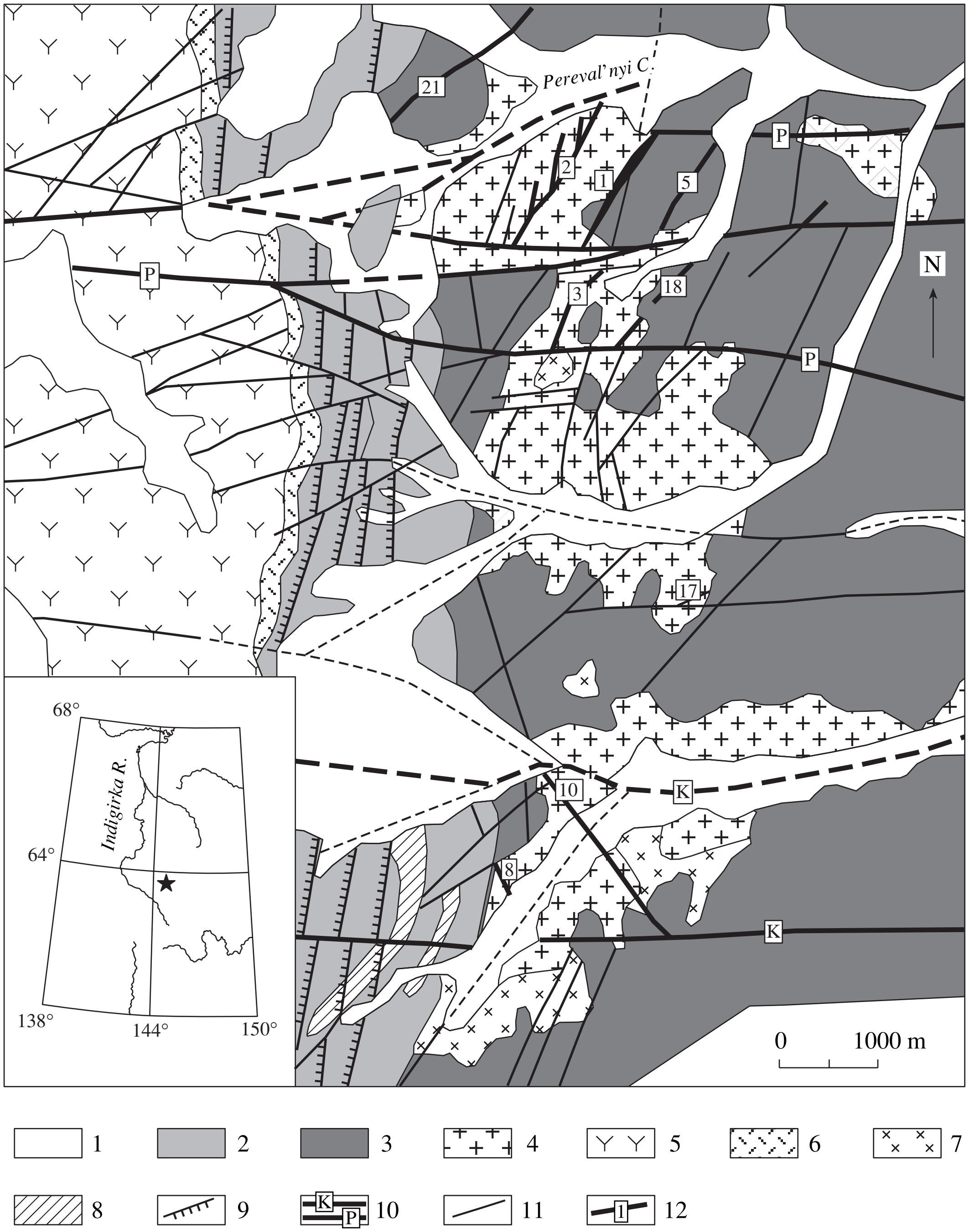

Fig. 3. Geological scheme of the Kupol'noe deposit. (1) Quaternary formation; (2) Jurassic terrigenous rocks; (3) Triassic terrigenous rocks; (4) Aptian granodiorite complex; (5) Neocomian dacite complex; (6) Beriassian rhyolite complex; (7) Volgain diorite complex; (8) gabbro-diabase complex; (9) faults; (10) Pereval'ninsk (P) and Kapriznensk (K) latitudinal fault zone systems; (11) tectonic faults; (12) ore bodies and their numbers.

The data obtained allow us to consider granites of the Trud and Kapriznyi massifs as derivates of granite magma that was generated at a temperature of 850–970°C under conditions of granulite facies, and was crystallized at a pressure less than 0.4–0.6 kbar (Shkodzinskii *et al.*, 1992).

Ore bodies of the Kupol'noe deposit are mainly located within the Trud and Kapriznyi granitoid massifs. In the hornfelzed sedimentary rocks of their exocontact zone, ore mineralization is less abundant.

Ore Bodies

About twenty ore bodies are found in two sectors (Kupol'nyi and Kapriznyi) of the deposit. Ore zones 1, 2, 3, 5, 8, 10, and 18 are explored down to depths of

100–350 m through drilling. Trenches and an adit more than 500 m long explored ore zone 1.

Ore bodies are controlled by repeatedly activated tectonic fractures. This led to a diversity and complexity of their morphology. Four morphological types of ore bodies have been recognized: (1) mineralized cataclastic zones; (2) lenslike veins; (3) stockwork zones; and (4) linear zones of disseminated ores.

Mineralized cataclastic zones are the predominant type of ore bodies in the deposit. Zones 1, 2, 5, and 18 are of this type. The largest among them is ore zone 1, which displays the northeastern (40°) strike. It occurs between the closely located subparallel sublatitudinal fractures (Fig. 3). The ore-bearing structure extends for more than 1300 m and its average thickness is about 8 m. Ore zone 1 consists of seven ore bodies. Only ore body 1 is traced along the whole extension of the ore-bearing structure. Other ore bodies are apophyses of this one or lenslike subparallel bodies.

Lenslike veins have a small thickness (5–70 cm) and length (20–50 m). They are located in both shear or tension fractures and wide fracture zones. They are composed, as a rule, of the consequently deposited mineral aggregates.

Stockwork zones occur rarely. These are a series of closely placed, thin (less than 5 cm) veinlets located in linear fracture zones or in large faults. The thicknesses of such zones vary from 1 to 6 m.

Linear zones of disseminated ores are intensely altered quartz–sericite rocks after granodiorites containing, in some places, abundant (up to 10–20 vol %) impregnations of pyrite, sphalerite, and galena.

METASOMATIC WALL ROCKS

Host rocks enclosing all types of ore bodies underwent metasomatic alteration around them. The metasomatic halos have a lenslike shape. Greisens, quartz–sericite rocks, and argillized rocks have been distinguished among metasomatic rocks. The quartz–sericite rocks (beresites) are most widespread among them.

Greisens

Several greisen zones, 30–50 cm thick on average and sometimes up to 2 m wide, occur along the southern contact between the Trud massif and hornfelses.

Chloritization of biotite and sericitization of plagioclase occur in an outer zone of the greisen halo. The amount of newly formed sericite that replaces chlorite and K-feldspar increases in the next zone. Newly formed quartz, replacing feldspar and sericite, and tourmaline appear as well.

The next zone consists of quartz, sericite, and tourmaline. The amount of sericite decreases in this zone, while the tourmaline fraction increases. Arsenopyrite and wolframite impregnation were observed in this zone.

Sericite disappears completely in the rear (inner) quartz–tourmaline zone. Quartz and tourmaline replace sericite. The arsenopyrite and wolframite amount increases in this zone by 1.2–2 times in comparison with the previous zone.

The major petrogenous components such as Al, Fe, Mg, Na, and K are removed at greisenization, while Si and S as well as Ca and Mn are gained in the rear zone. The Sn, As, W, and Bi content, as well as that of Co, Ni, and Cu increases from the outer zone to the rear one.

Quartz–Sericite Rocks

Quartz–sericite rocks replace biotite granodiorites, biotite granodiorite porphyries, and aplitelike leucocratic granites of the Trud and Kapriznyi massifs and, more rarely, hornfelses.

Quartz–sericite and carbonate-bearing quartz–sericite rocks are established among them. The carbonate-bearing quartz–sericite rocks occur at the area where vein mineralization is absent or occurs rarely.

Biotite is replaced by chlorite in an outer zone of the halo composed of both types of quartz–sericite rocks. Electron microprobe analyses indicate that chlorite contains 24.14–26.54 wt % SiO_2, 18.09–20.84 wt % Al_2O_3, 26.28–32.15 wt % FeO, 0.27–0.73 wt % MnO, and 9.3–14.59 wt % MgO. Calcite forms rims along chlorite aggregates.

An intense replacement of chlorite, calcite, and relic plagioclase by sericite and ankerite occur at the outer boundary of the next quartz–sericite–orthoclase–albite–ankerite zone of the quartz–sericite rocks. A complete disappearance of albite defines the inner boundary of this zone. The replacement of orthoclase by quartz and sericite is prolonged in the subsequent quartz–orthoclase–sericite zone.

Quartz is the principal newly formed mineral in the next quartz–sericite zone. It replaces rare relics of feldspars and sericite and fills in numerous cavities in mica aggregates.

The formation of monomineralic quartz rocks is observed at the contact with quartz veins. There is no clear boundary between quartz–sericite and quartz zone. The size of sericite aggregates decreases and the amount of metasomatic quartz increases gradually. Disseminated pyrite and arsenopyrite appear in the monomineralic quartz zone.

Chlorite and calcite are replaced by ankerite in the quartz–orthoclase–albite–sericite–ankerite zone which is followed by the carbonate-bearing quartz–sericite zone. Ankerite develops after albite, orthoclase, and plagioclase relics. Newly formed quartz and sericite replacing feldspars are encountered. The inner boundary is defined by a complete replacement of albite.

The replacement of orthoclase by quartz, sericite, and ankerite occurs in the quartz–orthoclase–ankerite zone.

Table 1. Average compositions of sericite from quartz–sericite and argillized rocks at the Kupol'noe deposit

Zone in halo	wt %							Coefficients in formula*							
	SiO_2	Al_2O_3	FeO	MgO	Na_2O	K_2O	Total	Si	^{IV}AL	^{VI}AL	Fe	Mg	Na	K	fen'
Quartz–sericite wall rocks															
1	48.34	32.46	1.43	1.02	0.29	9.96	93.50	3.24	0.76	1.80	0.08	0.10	0.04	0.85	0.21
2	47.18	32.93	1.40	1.29	0.11	9.92	92.83	3.19	0.82	1.80	0.08	0.13	0.02	0.85	0.19
3	46.65	31.84	2.41	1.31	0.10	10.02	92.40	3.19	0.81	1.76	0.14	0.13	0.01	0.88	0.21
4	45.78	32.22	2.49	1.08	0.14	10.23	92.00	3.16	0.84	1.78	0.14	0.11	0.02	0.90	0.18
Argillizite															
	49.19	32.83	0.53	0.70	0.04	7.94	91.23	3.27	0.73	1.84	0.03	0.07	0.01	0.68	0.19

Note: The zones of alteration halo are: 1—outer chlorite-bearing; 2 and 3—intermediate feldspar-bearing; 4—inner feldspar-free.

*The formula is calculated on the base of 11 atoms: Fen' = ((Si-3) + 0.5(3-ΣAl-Fe^{3+}) + (Mg + Fe^{2+}))/3, where Fe^{3+} = 1 + Al^{IV}-Al^{VI}-Ti, and Fe^{2+} = ΣFe-Fe^{3+} (atoms per formula).

Feldspars are nearly absent in the inner quartz–sericite–siderite zone. Fine-grained quartz is formed along the sericite aggregate margins in this zone. Carbonate is confined to the sericite aggregates. Its composition corresponds to minerals of the siderite series such as sideroplesite and magnooligonite.

Some changes of the sericite chemical composition were established in both types of quartz–sericite wall rocks (Table 1). Sericite from the outer chlorite-bearing zones contains the minimal concentration of Mg and Fe (zone 1, Table 1). This results in decreasing Al in tetrahedral coordination (^{IV}Al) to 0.76 atoms per formula. The ^{IV}Al content in this mineral from the intermediate feldspar-bearing zone is higher with 0.81–0.82 atoms per formula (zone 2 and 3, Table 1). Sericite from the inner feldspar-free zone of the halo contains 0.84 atoms per formula (zone 4, Table 1).

There is a systematic change of the carbonate composition from the outer to inner zone of quartz–sericite wall rocks (Fig. 4). Calcite containing low FeO and MnO (0.5 to 0.75 wt %) occurs in the outer zone. Carbonates of the dolomite–ankerite series are encountered in the intermediate zones of the carbonate-bearing quartz–sericite rocks. The Fe/(Fe + Mn + Ca + Mg) ratio increases in these minerals from the quartz–ankerite–albite–orthoclase–sericite zone to the quartz–ankerite–orthoclase–sericite one. Sideroplesite and mangansiderite with low MnO content are found in the inner quartz–siderite–sericite zone. The subsequent increasing in the Fe/(Fe + Mn + Ca + Mg) ratio toward the inner zone is observed (Fig. 4).

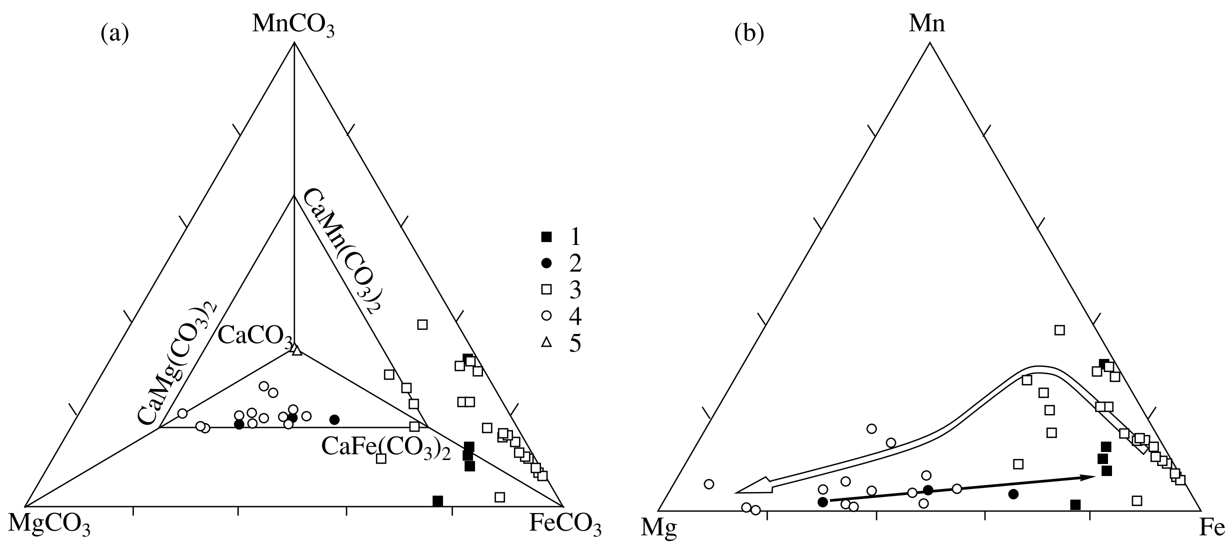

Fig. 4. Compositions of carbonates from the Kupol'noe deposit (a) and projection of compositions of carbonates (without calcite) onto Mg–Fe–Mn projection (b). (1) and (2) Carbonates of siderite–magnesite–rhodochrosite series: 1—metasomatic, 2—vein, (3) and (4) carbonates of dolomite–ankerite–kutnahorite series: 3—metasomatic, 4—vein, 5—calcite. The dark array shows an evolution of the composition of metasomatic carbonates toward inner zones of carbonate-bearing quartz–sericite wall rocks, while the white array indicates the evolution of carbonates from carbonate veins.

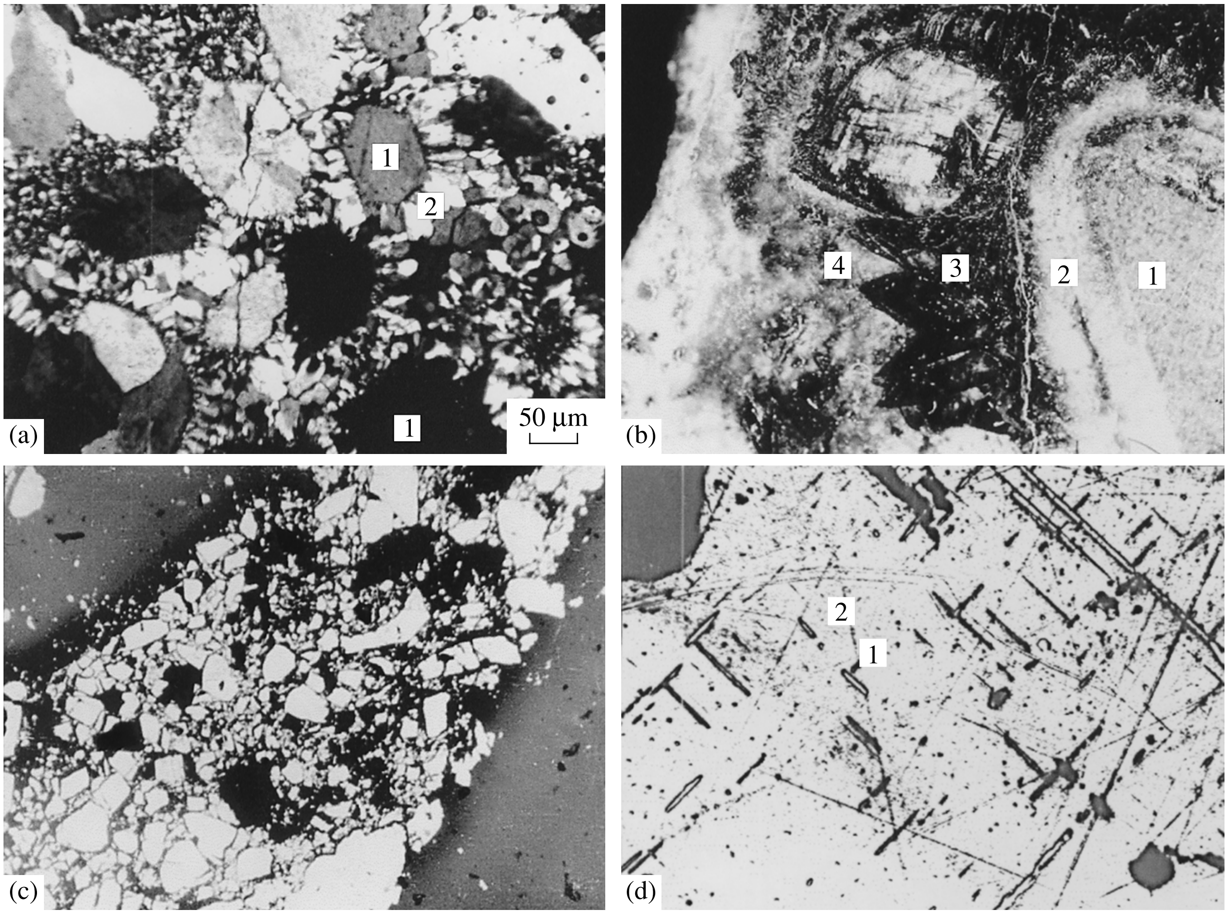

Fig. 5. Mineral intergrowths in ore bodies at the Kupol'noe deposit. a—Columnar aggregate of quartz IV grains (2) grow onto crystals of quartz III (1) thin section, crossed nicols; b—fragments of quartz–sericite rocks (1) with quartz rim (2) is overgrown with rhomblike crystals of siderite (3), zoned fine-grained quartz III (4) overgrows onto siderite; c—fine-grained quartz III cements cataclased arsenopyrite I, polished section, d—oriented lenslike ingrowths of diaphorite (1) in galena (2), polished section.

Argillized Rocks

Argillized rocks occur in ore zones 1 and 2 at their junction with latitudinal faults and in magmatic rocks only. The argillization zones are thin (less than 3 to 4 m) and are often overprinted on outer and intermediate zones of the quartz–sericite wall rocks.

Newly formed sericite replacing feldspars occurs in the intermediate zone of argillized halo. The chemical composition of sericite from argillized rocks is different from that of sericite quartz–sericite rocks. Lower Mg, Fe, and especially K contents and a higher Si content were detected in the first one (Table 1). X-ray diffraction has shown that the 1M polytype of sericite occurs in argillized halo.

The formation of kaolinite occurs with increasing alteration degree. Fine-grained quartz (about 0.01 mm) replaces sericite as well. The further alteration of the rock leads to a decrease in the hydromica amount, replaced by quartz and kaolinite. The interior zone of argillized halo is composed of quartz and kaolinite.

Argillization results in the removal of nearly all petrogenic components except Si. A SiO_2 content in the intermediate hydromica zone (calculated per a volume unit) remains constant, while that in the inner zones increases. Cu, Zn, and As are accumulated in rocks during argillization, while other elements are removed.

MINERAL COMPOSITION OF ORES

About 40 hypogenous minerals have been identified in the ore bodies of the Kupol'noe deposit. Quartz and carbonates are predominant minerals (more than 30 vol %). The major ore minerals (5–10 vol %) are galena, pyrite, and sphalerite. Sulfosalts are found in some areas of the ore bodies. Their content is less than 2 vol % on average. Four generations of quartz were established.

Quartz I is gray in color, cryptocrystalline, creasy and composes the inner zones of greisen metasomatic halo, veinlets in greisenized granodiorites, and the quartz–chlorite veinlets in hornfelses.

Quartz II is white, coarse-grained, and sometimes druslike. It composes veins and veinlets that bear tour-

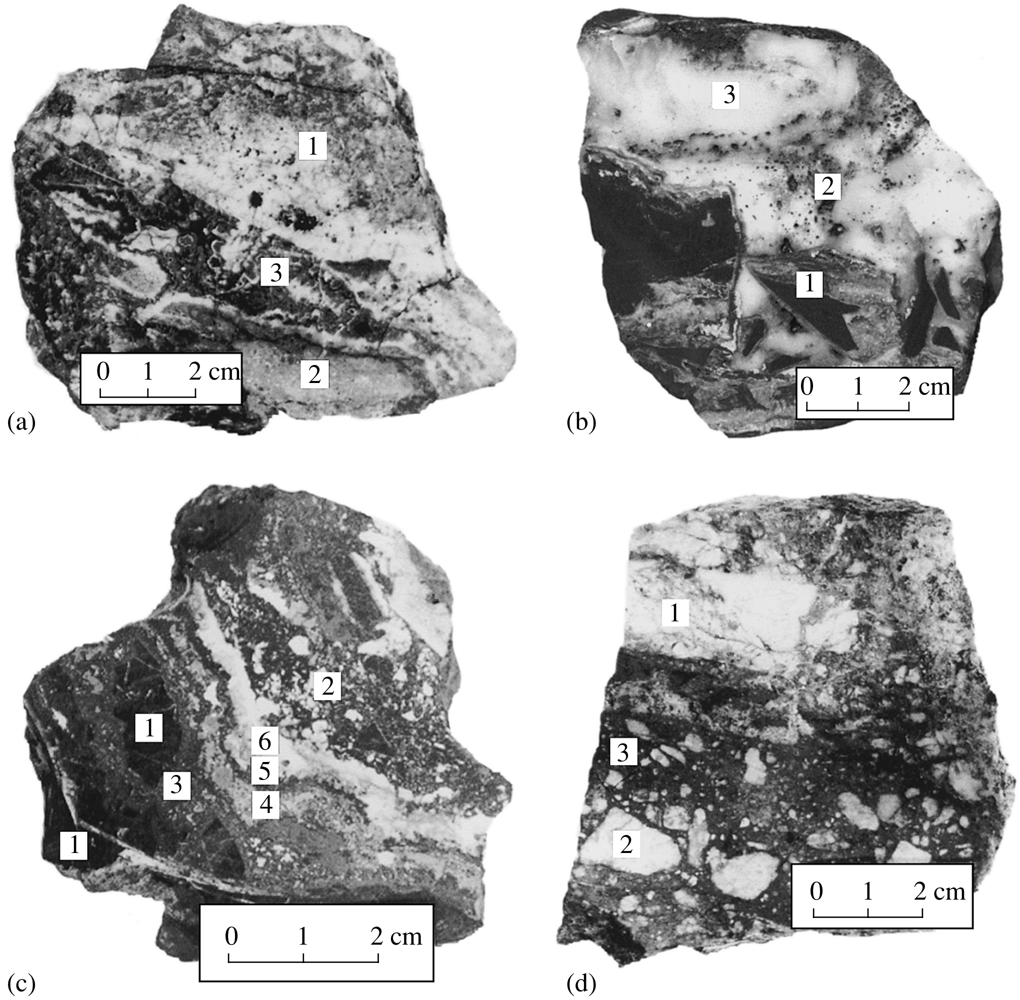

Fig. 6. Relationships of mineral aggregates in the Kupol'noe deposit, polished hand specimens. a—Altered granodiorite with spots and tiny veinlets of quartz I (1) and galena–sphalerite ore (2) are cross cut by veinlets of colloform–festoon quartz IV (3); b—fragments of siltstone with rims of rhythmically-zoned siderite (1) in cryptocrystalline quartz IV (2) with patches of pyrargirite, freibergite (dark) and calcite (3); c—fragments of hornfels (1) and milky-white quartz II (2) in sphalerite (3), sequential bands of siderite (4), galena (5), and fine-grained quartz III (6) overgrowing sphalerite; d—fragments of altered granodiorite (1) and milky-white quartz II (2) in grained quartz III saturated with tiny-grained aggregate of arsenopyrite II (3).

maline segregations, patches of coarse-grained arsenopyrite, disseminated wolframite and cassiterite. Spotted aggregates of quartz I in quartz II occur near vein selvages. Quartz II is cut by veinlets of siderite, galena, and its fragments are cemented by galena.

Quartz III is gray in color, translucent, and micrograined with well defined crystallographic shapes of grains that often display a zonation. Columnar aggregates of late quartz IV overgrow the outer zones of crystals (Fig. 5a). Small cavities, empty or filled with sulfosalts, are observed in quartz III, which bears galena and sphalerite patches and bands. Among the sulfide segregations, fine-crystalline aggregates of colorless tiny acicular cassiterite, tin- and silver-bearing minerals such as stannite, hocartite, franckeite, freibergite, andorite, etc. occur. Quartz III usually overgrows siderite (Fig. 5b), manganosiderite, and oligonite. Quartz III and ankerite form rhythmically banded aggregates. Quartz III and associated minerals are cut and cemented by quartz IV.

Quartz IV often forms cryptocrystalline aggregates with small lenslike cavities. Microspherolitic and zoned colloform sulfide aggregates overgrow walls of such cavities, while fine (less than 0.2 mm) sulfosalt crystals were found in their central parts. Quartz IV composes veinlets of 1–2 cm thick and thin (less than 30 cm) veins. Quartz IV cuts or cements mineral aggregates containing quartz I–IV (Fig. 6a, b). The disseminated ore minerals such as arsenopyrite, freibergite, pyrargyrite, Pb, Cu, and Fe sulfoantimonides, stibnite, marcasite, and rare sphalerite and galena occur in quartz IV. Dickite was found in cavities in quartz IV.

Cassiterite was observed in all ore bodies. Its content is from 0.1 to 3 vol %, and increases with depth. Two generations of this mineral were established.

Cassiterite I is represented by brown, sometimes zoned shortly-prismatic crystals up to 3 mm in size, and occurs in greisens adjacent to veins in intergrowths with muscovite and quartz. It is associated with druslike and massive quartz II, tourmaline, wolframite, and arsenopyrite I in quartz–tourmaline veins.

Cassiterite II forms spherolitic, "hedgehog-like" aggregates consisting of long-prismatic transparent crystals. Aggregate sizes are less than 0.2 mm, while those of individual crystals are less than 0.05 mm. Cassiterite II is intimately associated with fine-grained quartz, in which it forms monomineralic lenses. Cassiterite II occurs more often in sphalerite bands found in quartz. Overgrowth of cassiterite II on resorbed cassiterite I crystals was observed.

Wolframite is encountered in quartz–tourmaline veins as patchylike inclusions of 2–3 mm to 1.5 cm in size. The MnO content in this mineral is 1.6 to 2.0 wt %.

Carbonates

Early carbonates compose selvages in quartz–carbonate veins and veinlets (Fig. 5b). This evidences that they are earlier relative to quartz III. Often, carbonates form isolated rhomblike crystals or oval aggregates. They are overgrown by quartz III. Contents of components vary from 0 to 29.1 wt % CaO, 2.4–57.2 wt % FeO, 0.3–19.8 wt % MgO, and 0.2–22.2 wt % MnO. Carbonates with a high content of the siderite ($FeCO_3$) component are most widespread. Siderite, mangansiderite, sideroplesite, and oligonite were recognized among carbonates. Carbonates from early bands are compositionally close to carbonates from metasomatic wall rocks. The Mn content increases in carbonates from the subsequent bands. In some bands, it varies from 2 to 3 wt %. The difference in the MnO content between some bands is more than 5 wt %. In some carbonate samples, an increase of MnO content is accompanied with an increase of MgO content, while in most cases compositional data points lie along of the siderite–rhodochrosite series (Fig. 4).

Vein carbonates of dolomite–kutnahorite series are less widespread. More often they are observed in carbonate veins and veinlets. Socketlike and granular aggregates of these carbonates overgrow on manganosiderite aggregates and cavities in quartz. Zonal bands composed of carbonates of diverse tints and fabrics are also found. More rare carbonate veins with brecciated fabric, in which carbonates of the dolomite–ankerite series cement the siderite fragments, are observed. Individual veinlets of carbonates of this series are present in the intermediate zones of the quartz–sericite wall rocks. These carbonates are intimately associated with late sulfides. The ankerite–sphalerite intergrowths, carbonate patches with inclusions of galena, and chalcopyrite, and sulfosalt needles are often encountered.

The FeO and MgO ratios vary in carbonates of dolomite–ankerite–kutnahorite series, while CaO contents in them are constant. Zoned bands of carbonate aggregates differ in concentrations of these components. Later carbonates are dolomites in composition. Ankerite with high kutnahorite minal (up to 14–16 mol %) is usually confined to a boundary between the siderite and ankerite zones and contacts magnooligonite. A high Fe/(Fe + Mg + Mn) ratio of 0.4 is characteristic for these samples. A decrease of iron content in carbonates of dolomite–ankerite series is accompanied by a decrease of Mn concentration.

Calcite is the latest and less widespread carbonate. It fills intergranular spaces and cavities among early carbonates and quartz III and IV, and sometimes forms tiny microveinlets crossing these minerals. It is constant in composition and is characterized by low contents of FeO and MnO.

Sulfides

Galena is one of most widespread minerals in ore bodies. It was observed as impregnated grains and patches of up to 1–2 mm in size disseminated in fine-grained quartz and quartz–sericite wall rocks. Banded-impregnated fabrics are typical for thin (1–3 mm) galena bands. Massive ores contain galena grains up to 1–2 mm in size. Inclusions of different minerals in galena were observed. In galena bands located near the selvages of veins, sphalerite and cassiterite were encountered. In galena bands occurring close to the center of veins, stannite and freibergite are found. Franckeite and canfildite were identified in the latest galena rhythms. Inclusions of freibergite, diaphorite, franckeite, pyrargyrite, and miargyrite are randomly disseminated in massive galena. Electron microprobe analysis indicates that galena contains 1.2 wt % Ag, 4.7 wt % Sb, 0.89 wt % Bi, and 0.58 wt % Sn as trace elements.

Sphalerite is a widespread mineral as well. Two generations of this mineral were established.

Sphalerite I forms abundant impregnations in alteration halos and monomineralic bands in carbonate and quartz–carbonate veins (Fig. 6c). Sphalerite from disseminated ores contains inclusions of pyrrhotite, chalcopyrite, and rare stannite. In the near-selvage quartz bands from quartz–sulfide ores, abundant spherolitic inclusions of cassiterite occur in sphalerite. Bands containing abundant stannite follow them. Stannite forms tiny dissemination in some sphalerite zones and flamelike inclusions in sphalerite. Skeletal sphalerite grains were recorded among silver sulfoantimonides.

In rhythmically banded aggregates of sphalerite I, later bands are more light in color. The Fe content in sphalerite varies from 7.5 to 20.5 wt %. Sphalerite I contains from 0.11 to 0.75 wt % Cd, up to 0.59 wt % Mn, and up to 1.89 wt % Sn. The elevated Sn content in sphalerite is correlated with Cu content, which probably indicates the presence of submicroscopic stannite inclusions.

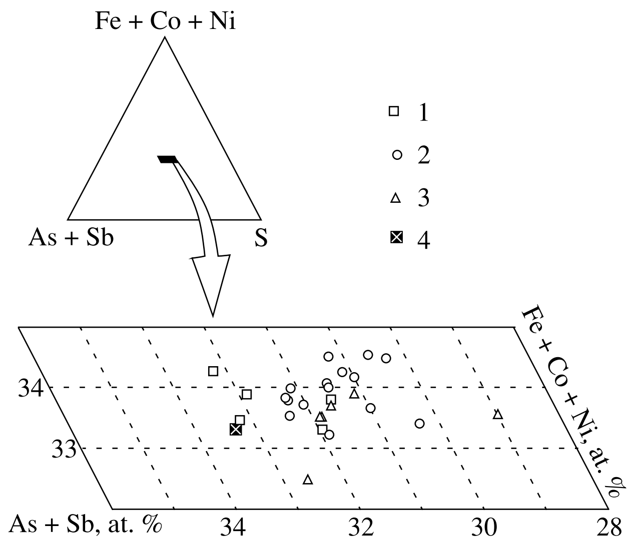

Fig. 7. Chemical compositions of arsenopyrite from the Kupol'noe deposit. (1) Arsenopyrite I, (2) arsenopyrite II, (3) arsenopyrite III, (4) composition of stoichiometric arsenopyrite.

Sphalerite II was observed as rare disseminated grains (up to 0.5 mm in size) in quartz IV near vein selvages. Fe content in this mineral varies from 0.3 to 7.2 wt %. It also incorporates 1.3 wt % Ag as an admixture.

Pyrrhotite is a rare mineral. Two generations of this mineral were distinguished. Pyrrhotite I is observed in hornfelses and in sulfidized granodiorites. Pyrrhotite occurs rarely in veins in association with sphalerite and galena.

Chalcopyrite is found in association with pyrrhotite from hornfelses and granodiorites. In veins, chalcopyrite is present in association with pyrrhotite, more rarely with sphalerite, stannite, and galena, and as emulsion inclusions in sphalerite.

Stannite occurs in veins and quartz–sericite wall rocks. This mineral is intimately associated with sphalerite, whose zoned grains contain abundant tiny inclusions of stannite. It replaces resorbed grains of cassiterite I as well. Stannite contains iron from 10.3 to 12.6 wt %. Admixtures of zinc and silver are detected in this mineral. The silver content ranges from 0.4 to 5.8 wt %.

Stibnite is a relatively rare mineral. It is intimately associated with quartz IV and forms patches in the columnar-laminar aggregates. The mineral was observed as euhedral intergrowths with native antimony and hypogenic valentinite. It is formed together with reniform-zoned aggregates of marcasite at replacement of berthierite.

Marcasite and pyrite usually occur in association with each other. Pyrite–marcasite aggregates are concentrated in cryptocrystalline quartz IV in massive sulfide ores and rarely in carbonate–quartz veins. A pseudomorphic replacement of siderite and tiny veinlets running along cleavage in siderite are found in these veins. Pyrite occurs separately from marcasite in quartz–sericite wall rocks in the form of cubic metacrysts. Pyrite contains up to 1.44 wt % As.

Arsenopyrite is represented by three generations.

Arsenopyrite I forms coarse-grained aggregates in zones of greisens and in massive and druslike milky-white quartz. These aggregates are cataclased and cemented by quartz III (Fig. 5c) bearing disseminated sulfides, as well as by quartz IV. The replacement of arsenopyrite I by silver sulfosalts was observed. Rims of late arsenopyrite II around early arsenopyrite I were also found. The composition of this mineral fluctuates (Fig. 7): As content ranges from 42.9 to 46.0 wt % or from 31.1 to 34.0 at. %. It contains up to 1.01 wt % Co and 0.1–0.2 wt % Ni.

Arsenopyrite II was observed as fine-grained intergrowths of rhomblike euhedral grains in quartz III. It forms tiny lenses along contacts of quartz veinlets and disseminated metacrysts in quartz–sericite wall rocks.

The composition of arsenopyrite II varies (Fig. 7): As content ranges from 40.3 to 44.3 wt %. An admixture of 2.9 wt % Sb and Co up to 1.9 wt % was detected. Some grains contain up to 0.4 wt % Ni. The mineral is characterized by high sulfur content in comparison to the stoichiometric formula of FeAsS: the (As + Sb)/S ratio is <0.93. Of other significant trace elements, Pb, Zn, and Sn (up to 0.3 wt %) were detected.

Arsenopyrite III occurs as fine-crystalline aggregates. Grains possess prismatic and impressed rhomblike shape. This mineral is intimately associated with quartz IV. Arsenopyrite III overgrows aggregates of arsenopyrite I and II and scorodite, which contains arsenopyrite II relics. Possibly, this indicates that an arsenopyrite II oxidation preceded the deposition of arsenopyrite III.

Arsenopyrite III varies in composition (Fig. 7). The As and Sb content in this mineral ranges from 35.7 to 44.5 wt % and from 0.23 to 9.32 wt %, respectively. A zonal distribution of high Sb concentration in the arsenopyrite grains was established. A Co content of up to 3.8 wt % was detected in zones with a high Sb concentration. Higher sulfur content and Fe deficit, relative to the stoichiometric formula of FeAsS, were found. Apparently, this evidences the true compositional variation of this mineral and is not a result of systematic analytical errors (Bortnikov, 1993).

Sulfosalts

High contents of sulfosalts at the deposit often define the economic value of ore bodies.

Tetrahedrite and freibergite[1] are major silver-bearing minerals of the deposit. Maximal sizes of these minerals are <3–5 mm in cavities of quartz. Tetrahe-

[1] Mineral containing more than 3.8 atoms of silver per formula is referred to freibergite.

drite occurs in intimate intergrowths with galena, stannite, and, more rarely, with pyrargyrite. No evidence for replacement between these minerals was found, indicating their coeval crystallization. However, younger tiny veinlets of pyrargyrite were observed in these minerals. Tetrahedrite is often associated with sphalerite. It was deposited later than sphalerite, and commonly overgrows its grains, without any signs of replacement relationships. In contrast, a replacement of sphalerite by freibergite is clearly observed. The freibergite rims are formed around sphalerite grains. Sometimes, a sphalerite grain is almost completely replaced. Freibergite with silver content >40 wt % is encountered in ores of the deposit (Table 2). It is younger than tetrahedrite and grains and their aggregates, which are overgrown and cut by freibergite. Minerals are easily distinguished under a microscope due to different relief and tint.

The chemical compositions of the minerals of the tetrahedrite–freibergite series, $(Cu, Ag)_{10}(Fe, Zn)_2(Sb, As)_4S_{13}$, vary considerably (Fig. 8). They contain 13.52–50.41 wt % Ag, 0.25–27.62 wt % Cu, 0.5–3.86 wt % Zn, and 3.09–6.51 wt % Fe. Some grains contain up to 4.82 wt % As and 1.37 wt % Sn. Silver prevails over copper in most analyzed grains.

Silver sulfoantimonides: miargyrite, pyrargyrite, and stephanite are principal silver minerals in the deposit. Miargyrite prevails among them. These minerals occur as intimate ingrowths with each other. Pyrargyrite is found in cavities in ankerite, where it forms crystals 3–4 cm in size. Pyrargyrite and miargyrite are often encountered in association with galena. They overgrow each other, filling cavities.

The chemical compositions of the silver sulfoantimonides are variable. Copper amounting to 5.4 wt % was detected in miargyrite. Bi admixture was found in some grains of these minerals.

Silver and lead sulfoantimonides are diaphorite, owyheeite, and andorite IV (Fig. 9).

Diaphorite ($Pb_2Ag_3Sb_3S_8$) and *andorite IV* ($PbAgSb_3S_6$) are disseminated in galena. Their oval inclusions in the galena aggregates are randomly distributed, and fine lenslike inclusions are confined to cleavage in the host mineral (Fig. 5d).

Results of electron microprobe analysis evidence the compositional variations in diaphorite that are compatible with the homogenization field found for its synthetic analogue (Bortnikov *et al.*, 1980).

Data points from electron microprobe analysis of andorite IV are located around a figurative point of the theoretical composition of this mineral, which corresponds to $PbAgSb_3S_6$. A deviation of the *N* value (3.88–4.28) from theoretical was found (Table 3, analyses 1–6). It characterizes a number of octahedrons in galena-like slab in the crystal structure of this mineral (Makovicky and Karup-Møller, 1977). The content of the andorite component ranges from 89.2 to 98.9%. The following contents of Fe and Sn were detected in andorite: 0.55–0.9 wt % and 0.57–1.54 wt %, respectively.

Table 2. Chemical compositions of freibergite from the Kupol'noe deposit (wt %)

Number under the order	Ag	Cu	Fe	Zn	Sb	S	Total
1	50.41	0.25	4.82	0.95	23.81	20.07	100.31
2	49.35	1.02	4.37	0.91	22.63	20.44	98.72
3	50.83	1.27	4.75	0.77	23.20	18.57	99.39
4	50.13	1.19	4.07	0.61	24.07	19.56	99.63
5	49.91	1.30	4.03	0.91	24.59	19.03	99.77

A bismuthian variety of andorite, in which antimony is substituted for bismuth, was identified (Table 3, analyses 7 and 8). Their empirical formulas are as follows: $Ag_{0.73}Pb_{1.49}Sb_{1.91}Bi_{0.80}S_{6.07}$ and

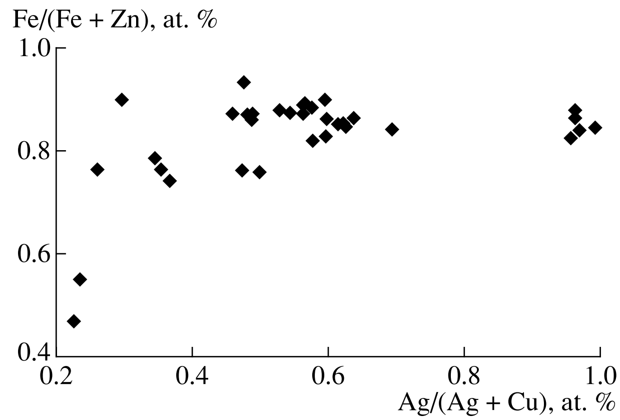

Fig. 8. Fe/(Fe + Zn) vs. Ag/(Ag + Cu) plot for tetrahedrite–freibergite minerals from the Kupol'noe deposit.

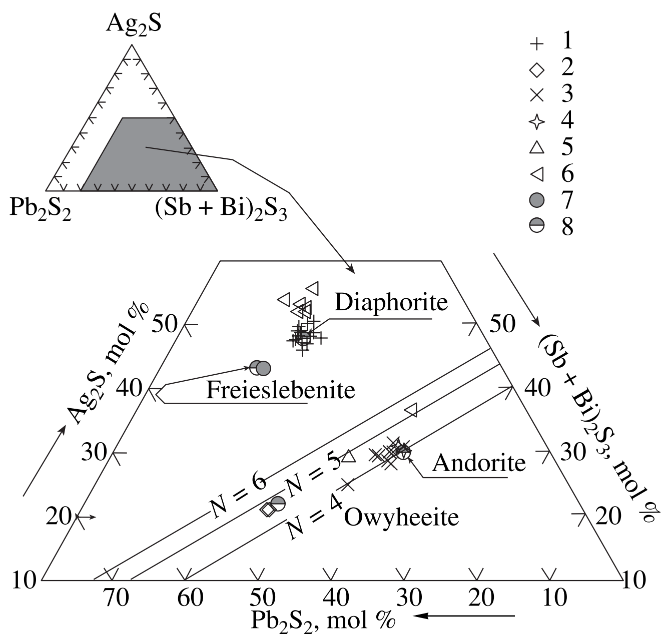

Fig. 9. Chemical composition of lead and silver sulfosalts from the Kupol'noe deposit. (1) Diaphorite, (2) owyheeite, (3) andorite, (4) Sb–gustavite, (5) phase III, (6) unnamed phase, (7) freieslebenite, (8) theoretical compositions.

Table 3. Chemical compositions of lead and silver sulfosalts from the Kupol'noe deposit (wt %)

Number under the order	Sample number	Ore zone number	Mineral	Ag	Cu	Fe	Pb	Sb	Bi	Sn	S	Total	N	x
1	185–86	10	Andorite	11.24	N.d.	0.76	23.07	41.23	N.d.	0.57	21.72	98.59	3.88	94.72
2	53–63	10	″	11.38	″	0.55	22.65	40.65	″	1.25	21.96	98.44	3.98	93.43
3	53–63	10	″	11.89	″	0.71	22.92	39.87	″	1.54	22.2	99.13	4.28	89.15
4	187–86	10	″	12.47	″	0.74	19.9	41.8	″	0.96	22.58	98.45	4.05	98.87
5	185–86	10	″	12.56	″	0.89	21.24	41.29	″	1.14	22.06	99.18	4.23	93.71
6	185–86	10	″	12.63	″	0.9	21.09	41.77	″	0.99	22.14	99.52	4.18	95.06
7	177–123	2	Bi–andorite	8.11	″	N.d.	31.72	23.86	17.12	N.d.	19.97	100.78	3.99	74.40
8	177–123	2	″	8.66	1.33	″	25.61	24.68	19.13	″	20	99.41	4.38	88.20
9	61–88	2	III	9.02	1.19	″	30.17	25.58	14.49	″	19.2	99.65	4.96	78.20
10	177–123	2	Unnamed	12.68	0.81	″	16.21	13.37	36.29	″	18.56	98.92	5.42	99.37
11	177–123	2	Sb–gustavite	10.9	N.d.	″	20.18	13.42	36.92	″	19.43	100.85	4.22	97.84
12	177–123	2	″	10.4	″	″	19.3	11.86	39.37	″	19.45	100.38	4.02	100.81
13	1–803	1	Unnamed	28.47	″	″	24.54	25.48	N.d.	″	19.38	98.56	–	–
14	94–86	1	″	27.94	″	″	28.39	25.09	0.22	″	18.33	99.86	–	–
15	535–87	1	″	27.88	″	″	29.98	22.74	N.d.	″	17.94	98.54	–	–
16	541–10	2	″	27.84	″	″	28.05	26.25	″	″	17.82	99.96	–	–
17	180–86	10	″	27.47	″	″	29.04	25.25	″	″	18.35	100.11	–	–
18	202–69	21	″	27.53	″	″	28.5	26.55	″	″	17.43	100.01	–	–

Note: $N = -1 + \left(\frac{1}{Sb_i + \frac{Pb_i}{2}} - 0.5\right)$; $x = 1 - \frac{2Sb_i - Pb_i - 1}{6\left(\frac{Pb_i}{2} + Sb_i - \frac{5}{6}\right)}$ (according to Makovicky). N.d.—not detected.

$Ag_{0.77}Cu_{0.20}Pb_{1.19}Sb_{1.95}Bi_{0.80}S_{6.0}$. Calculated N values are equal to 3.99 and 4.37, and x (a fraction of the andorite component) is 74.4% and 88.2%, respectively.

Owyheeite ($Pb_{10}Ag_3Sb_{11}S_{28}$) is rarely encountered as needle inclusions in ankerite. Its composition is depleted in silver in comparison to its theoretical formula, but falls in the compositional homogenization field of this mineral (Moelo *et al.*, 1984).

Some Ag–Bi–Pb–Sb–sulfosalts found were not identified. Possibly, they are unknown members of the lillianite homologous series (Table 3, analyses 9 and 10). Calculated values of N and x (a fraction of the gustative component) vary from 4.96 to 5.42 and 78.2 to 99.4%, respectively. One of them corresponds to phase III (Table 3, analysis 9) and was discovered by Mozgova *et al.* (1989), while the second one (Table 3, analysis 10) has no analogues.

The antimony-bearing sulfobismuthides of lead and silver were found in a veinlet of manganosiderite as tiny inclusions containing pink grains of native bismuth. Among their aggregates, Ag-tetrahedrite and stannite were observed. The principal mineral among sulfobismuthides is characterized by lower reflection and noticeable bireflection. Other, more light, phases are observed as tiny inclusions. The silver sulfobismuthides are encountered in association with galena and silver sulfoantimonides. Results of electron microprobe analysis of the principal phase (Table 3, analyses 11 and 12) correspond to Sb–gustavite, $PbAg(Bi, Sb)_3S_6$. Bismuth in these minerals is substituted for antimony. Calculated values of N and x (a fraction of the gustavite component) are equal to 4.22 and 4.02, and 97.84 and 100.81%, respectively, and correspond to the idealized values for gustavite (Makovicky and Karup-Møller, 1977).

Several grains of lead and silver sulfoantimonide that were not previously described (Table 3, analyses 13–18) were encountered in ores of the deposit. This mineral contains more silver relative to that found in diaphorite.

Sulfostannates

Sulfostannates found in the deposit are franckeite, hocartite, and canfildite, which are intimately intergrown with each other.

Hocartite (Ag_2SnFeS_4) is the most widespread sulfostannate mineral. It forms relatively large (up to 1 cm) aggregates filling in cavities in quartz III. It is most often associated with galena occurring as inclusions in hocartite. Corroded relic grains of cassiterite were found among its aggregates. Its composition and X-ray powder diffraction pattern correspond to the reference data (Nekrasov *et al.*, 1978).

Canfildite (Ag_8SnS_6), associated intimately with stannite and franckeite, is rarely encountered in ores of the deposit. It was deposited later than stannite as it overgrows this mineral and penetrates into its grains along microcracks. Canfildite contains trace concentrations of Se (0.4–0.5 wt %) and, more rarely, Te (1.6 wt %).

Franckeite, $Fe(Pb, Sn)_6Sn_2Sb_2S_{14}$ occurs in association with cassiterite. The franckeite aggregates containing the relic grains of cassiterite occur more often in galena. Curved laminar aggregates and single lamina of franckeite are usually replaced by cassiterite along their margins and form inclusions in galena.

The chemical compositions of franckeite range from 48.97 to 53.77 wt % Pb, from 10.7 to 11.82 wt % Sb, from 10.56 to 13.66 wt % Sn, from 0.21 to 1.33 wt % Ag, and from 2.06 to 2.62 wt % Fe. Trace amounts of Cu (0.81 wt %) were detected in some franckeite samples. Results of electron microprobe analysis lie within the compositional homogenization field of franckeite.

Lead sulfoantimonides: boulangerite ($Pb_5Sb_4S_{11}$) *and jamesonite* ($FePb_4Sb_6S_{14}$) are considered to be latest minerals. They form disseminated inclusions in ankerite. Boulangerite was found in calcite as well. Trace contents of Bi amounting to 1.08 wt % and Ag up to 2.16 wt % were detected. Jamesonite contains 0.48 wt % Bi and 0.33 wt % Sn.

Chalcostibite ($CuSb_2S_4$) is a rare mineral. It usually forms separate laminar grains. Small fine aggregates are present in druslike quartz.

Berthierite ($FeSb_2S_4$) *and gudmundite* (FeSbS) occur in quartz IV in association with stibnite. Acicular aggregates of berthierite with inclusions of gudmundite overgrow colloform quartz. Berthierite is replaced by stibnite and marcasite aggregates.

MINERAL FORMATION SEQUENCE AND MINERAL ASSEMBLAGES

Diversity in textures and structures of ores evidence a complicated dynamic environment of ore formation and their hypogenous recrystallization.

Massive, druslike, and patchy fabrics of ores are recorded in veins of gray metasomatic quartz and milky-white arsenopyrite-bearing quartz. Banded fabrics, mainly composed of carbonates, quartz, and sulfides (Fig. 6c) are widespread. Multiple alternation of siderite, sphalerite, and galena bands was observed. The alternation of bands composed of the same mineral (carbonate, quartz, or sphalerite), but different in color, grain, shape, or size was recorded too.

The cataclastic and cementation fabrics are widespread as well (Fig. 6b and d). They indicate that the ore formation occurred in dynamically active faults. The repeated opening of fractures caused the multiple cataclasis of mineral aggregates and led to the formation of complex brecciated textures (Fig. 6a). Fragments of milky-white quartz II and granodiorites are cemented by fine-grained, and rarely, druslike quartz III bearing galena and sphalerite. Fragments of these aggregates are included in cryptocrystalline or zoned-colloform quartz IV.

Crossing and cementation of milky-white druslike quartz II by the quartz–carbonate–galena veins and veinlets, and then by cryptocrystalline and zoned-colloform quartz IV (Fig. 6a), occur very often, while all the earlier aggregates are cut by veinlets of hypogenous jarosite.

Mineral intergrowths in ores are also diverse. Euhedral texture of milky-white quartz and fine-grained quartz, arsenopyrite and sphalerite, and enhedral intergrowths of jarosite and quartz are widespread. Sphalerite and ankerite were coevally crystallized form euhedral textures. Mutual boundary intergrowths usually characterize the co-crystallization of two or three minerals: freibergite and galena, stannite and chalcopyrite, pyrargyrite and galena, and freibergite, stannite, and pyrargyrite. Poikilitic ingrowths of galena in miargyrite are common.

The sequential precipitation of minerals is clear at filling in open spaces with the crystalline aggregates of gangue minerals such as quartz and siderite. The open spaces in these minerals are, in turn, filled in by later gangue and opaque minerals. Spherolite and cockade texture are typical as well.

The study of the spatial distribution, temporal relationships, and textural and structural features among different mineral aggregates and metasomatic alterations of enclosing rocks suggests that the deposit has been formed as a result of repeated hydrothermal activity. This led to the spatial telescoping of three types of mineralizations, namely rare metal (tin–tungsten), tin–silver–base metal, and silver–antimony mineralizations. The different mineralizations are confined to the different tectonic fractures. Each of them is characterized by the definite combination of the mineral assemblages and is accompanied by the metasomatic alteration that is intrinsic to a certain mineralization type only.

Rare Metal Mineralization

The rare metal (tin–tungsten) mineralization is controlled by sublatitudinal and northeasterly-trending faults, and is the early one. The sublatitudinal faults control zones of intense greisenization of host rocks which resulted in the formation of quartz–muscovite halos in granodiorites and tourmaline–quartz halos in hornfelses, while the northeasterly-trending faults enclose cassiterite–arsenopyrite veins and veinlets.

Tin–Silver–Base Metal Mineralization

The tin–silver–base metal mineralization is exclusively located in the northeasterly- and northwesterly-trending faults. This mineralization was formed after intense fracturing of rare metal mineral aggregates. An intense development of the quartz–carbonate–pyrite–sericite wall rocks preceded the formation of the tin–silver–base metal mineralization. Then, the crystallization of carbonates filling open fractures occurred. The rhythmically banded fabrics of veins are caused by the alteration of the variously colored zones and compositionally different carbonates. These minerals are the earliest ones among the tin–silver–base metal mineralization. They are usually located near selvages of veins. Sometimes, they occur as individual veinlets at flanks of ore bodies in places of their pinching out. This assemblage is followed by that of cassiterite–arsenopyrite–quartz (Fig. 5b). The finding of fragments of manganosiderite and rare tiny veinlets of quartz III in the quartz–arsenopyrite–quartz mineral aggregates indicates a local intraore cataclasis.

The chalcopyrite–sphalerite–galena–quartz assemblage was formed later and overgrows their rhythmically banded cassiterite–arsenopyrite–quartz aggregates. The following sequence of bands is characteristic of banded mineral aggregates: cassiterite–sphalerite–quartz one $\longrightarrow$ galena–sphalerite–quartz one $\longrightarrow$ quartz–chalcopyrite–stannite–sphalerite–galena one $\longrightarrow$ chalcopyrite–stannite–sphalerite–galena one. Each of them is considered as a single paragenetic mineral assemblage. A gradual decrease of the sphalerite role, an increase in galena, and an appearance of carbonate are established toward late bands. Changing in the chemical composition of minerals inside the bands was also recorded. Thus, the Fe and Mn contents decrease in sphalerite. The Ag concentration increases in stannite and galena. It was found that early mineral aggregates are more widespread at deep levels, while latest mineral aggregates are more abundant at upper levels. Galena is the predominant mineral at upper levels. Sphalerite dominates at deep levels of ore zones 1, 2, and 18.

The galena–freibergite–pyrargyrite assemblage composes, as a rule, central parts of ore bodies. Diaphorite, miargyrite, and ankerite are quite often in this assemblage. Increasing of the amount of these minerals improves the economic value of the ores. In some places silver grade amounts to 3–6 kg/t.

The crystallization of the marcasite–ankerite assemblage completes the formation of this mineralization.

In general, the deposition of minerals from this style of ores occurred after the following scheme of: oxides–sulfides–silver sulfosalts–tin and silver sulfosalts–sulfides–oxides. The crystallization of carbonates begins and completes the process of the formation of the tin–silver–base metal ores.

Silver–Antimony Mineralization

Silver–antimony mineralization is mainly located in the sublatitudinal faults and in diagonal fracture system adjacent to sublatitudinal faults. As a rule, it is spatially separated from earlier mineral aggregates. Rare metal and tin–silver–base metal mineralizations are cut and cemented by silver–antimony mineral aggregates, being telescoped on each other. The silver–antimony mineralization was formed after intense cataclasis and fracturing of mineral aggregates described above. As a result, the brecciated fabrics originated because fragments of rare metal ores were cemented with the silver–base metal aggregates, which, in turn, were cemented by quartz–sulfosalt aggregates. The argillization preceded the formation of silver–antimony mineralization, while at deep levels, adularization accompanied this ore type. These processes were most intensive at overprinting onto the quartz–sericite wall rocks, and unstable under new conditions. The filling of veins by silver–antimony ores commenced with the formation of arsenopyrite–marcasite–quartz association. Quartz composes nearly 99 vol % of these veins. The zoned-colloform and combshaped-festoon fabrics are typical of this quartz. Fine arsenopyrite crystals are disseminated near vein selvages. Rare plate aggregates of marcasite are encountered across the complete vein thickness. There was a tendency in changing of arsenopyrite + marcasite + quartz mineral aggregates through the marcasite + quartz aggregates to quartz aggregates in an upward direction.

The galena–pyrargyrite–freibergite association forms small patches in quartz–arsenopyrite–marcasite veins. They occupy about 0.5 vol %. Cryptocrystalline and fine druslike quartz (up to 30 vol %) was found in disseminated freibergite–pyrargirite aggregates. Silver grade amounts are 2–4 kg/t in such areas.

The stibnite–berthierite–calcite assemblage occurs very rarely. Calcite is a predominant mineral, while boulangerite and chalcostibite are found sporadically. Calcite is often separated from sulfides and sulfosalts. This assemblage fills open spaces in the quartz vein.

The quartz–dickite–jarosite assemblage is encountered in small cavities and forms veinlets of <10 cm thick crossing, and sometimes cementing, early-deposited mineral aggregates.

FLUID INCLUSIONS

Fluid inclusions in quartz of different generations were studied. Microthermometric measurements were carried out on doubly polished wafers using techniques described by Borisenko (1977). One hundred thirty-four individual fluid inclusions from 12 specimens were examined.

Characterization of Fluid Inclusions

Three types of fluid inclusions were distinguished according to their phase composition at a room temperature. Type I are two-phase (L < V) fluid inclusions filling mainly with vapor phase. Their sizes are 15 to 5 μm and less. Type II are two-phase inclusions containing liquid and a vapor bubble, where the liquid phase prevails over the vapor phase. Type III are three-phase fluid inclusions containing solid (>5 μm), liquid, and vapor phases. The simultaneous entrapment of fluid inclusions characterized by variable ratios of liquid and vapor phases is possible evidence for vapor phase separation from mineral-forming fluids (Roedder, 1984).

Primary and secondary fluid inclusions were recorded. Primary inclusions are those that are clearly confined to the definite crystallographic planes of the mineral-host, to growth zones in quartz, and randomly distributed over grains of this mineral (Ermakov, 1972; Roedder, 1984). Fluid inclusions healing cracks in quartz were referred to the secondary fluid inclusions. Special attention was paid to the examination of primary inclusions in minerals.

Quartz I and II contain abundant fluid inclusions of types I and II. Small type III fluid inclusions (5–15 μm) are often encountered in these minerals. The solid phase found in them is identified as halite. Sometimes, they contain poorly soluble enhedral solid phase of tabular or plate shapes. The secondary inclusions are mainly found in quartz I and II. Clusters of primary fluid inclusions were found in these minerals as well. Type I and III fluid inclusions were recorded in the same growth zones of quartz crystals. This is evidence for their simultaneous entrapment. In turn, this indicates that quartz I is crystallized from a "boiling" fluid (Bodnar *et al.*, 1984). Sometimes a zoned distribution of primary fluid inclusions is distinguished in small crystals of early quartz (specimens 221-86). Usually they are referred to the type II fluid inclusions.

The zoned distribution of fluid inclusions was found in the individual crystals of quartz III (Fig. 10). The inner zones of crystals contain relatively large (up to 20 μm in size) pseudosecondary and primary two-phase fluid inclusions. These fluid inclusions are located separately from each other or as clusters of several fluid inclusions. The outer zones are densely saturated with small primary fluid inclusions. Their sizes are, as a rule, less than 15 μm along a long axis.

Quartz IV contains two-phase fluid inclusions and displays the zoned structure as well.

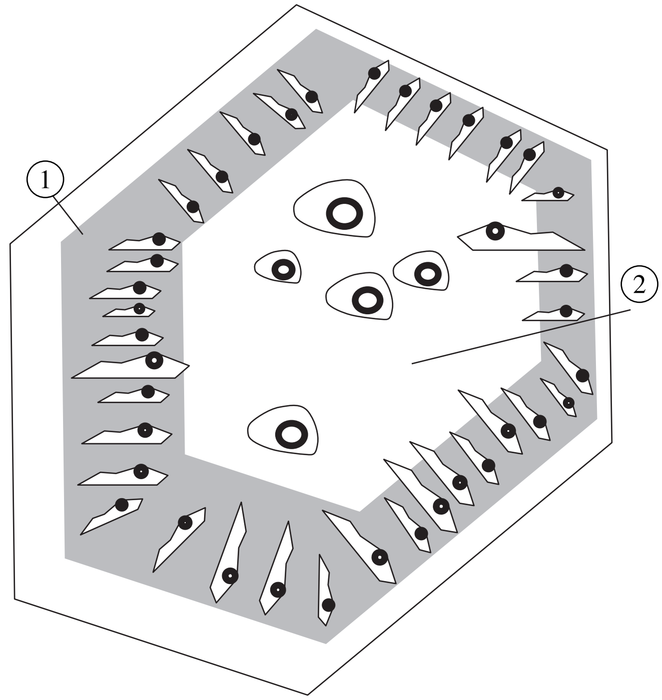

Fig. 10. Zoned distribution of fluid inclusions in crystals of quartz III. (1) Outer zone, (2) inner zone.

Microthermometric Measurements

Heating of fluid inclusions has shown that the general temperature range of homogenization of fluid inclusions is from 125 to 450°C (Table 4, Fig. 11). Type I and III fluid inclusions in early quartz were homogenized at higher temperatures varying from 285 to 450°C. It should be noted that the type I and III fluid inclusions containing solid phase were homogenized at the same temperature. This indicates the deposition of quartz I from the "boiling" fluid as well. Lower homogenization temperatures of 150 to 225°C were measured for the type II fluid inclusions from specimens of zoned crystals of quartz (samples 221-86). Possibly, these zones are relatively late generations of quartz overgrowing earlier quartz. In this case, the measured temperatures characterize the temperatures of the entrapment of a late fluid.

Fluid inclusions in quartz III and IV are homogenized at 125 to 210°C and 135 to 280°C, respectively (Table 4, Fig. 11). A decrease in the homogenization temperature of fluid inclusions from the inner zones to the outer ones was recorded.

Type III fluid inclusions contain high-concentrated chlorine solutions that follows from the occurrence of salt solid crystals in them. The low eutectic temperatures of –66 to –62°C indicate the presence of a noticeable $FeCl_2$ amount in addition to NaCl that predominates in solution (Borisenko *et al.*, 1990, 1997; Borovikov, 1995). The total salt concentration of the capsulated solutions was estimated using melting temperature of freezed phase (Borisenko, 1977). No replacement of halite by the NaCl crystallohydrate was observed. Thus, a solid phase crystallized at freezing of fluid inclusions was conditionally identified as ice.

Table 4. Results of the microthermometric study of fluid inclusions in quartz from silver ores of the Kupol'noe deposit

Number under the order	Sample number	Generation	Phase composition	Homogenization temperature, °C		Melting temperature, °C		Concentration, wt % NaCl-equiv
				vapor	halite	eutectic	ice	
1	186–69	1.2	L < V	400–450(7)	–	–64…–62(7)	–3…–2	4.9–3.3
2	186–69	1.2	L + V + S	440–290(14)	315–255(14)	–64…–62(5)	~–40	~36–38
3	188–69	1.2	L + V + S	310–285(12)	265–255(12)	–66…–64(6)	~–40	~36
4	221–86	1.2	L + V	225–150(7)	–	–44…–42(6)	–5…–4	7.9–6.4
			L + V	155–150*(7)	–	–	–	–
5	114–2–86	3	L + V	210–205(5)	–	–36…–34(6)	–3…–2	4.9–3.3
6	196–86	3	L + V	185–140(18)	–	–34…–32(7)	–6…–5	9.2–7.9
7	195–86	3	L + V	175–165(12)	–	–34…–32(5)	–5…–4	7.9–6.4
			L + V	135–125*(5)	–	–	–	–
8	535–87	3	L + V	140–150(4)	–	–34…–32(3)	–3…–2	4.9–3.3
9	458–87	4	L + V	250–280(11)	–	–36…–34(7)	–5…–4	7.9–6.4
						(–58…–57)**		
10	529–87	4	L + V	180–170(9)	–	–34…–32(8)	–4…–3	6.4–4.9
			L + V	155–135*(6)	–	–	–	–
11	127–86	4	L + V	175–160(6)	–	–38…–36(6)	–3…–2	4.9–3.3
12	160–69	4	L + V	168–135(11)	–	–36…–35(6)	–5…–4	7.9–6.4

Note: The number of measurements is given in brackets.
* Fluid inclusions from outer zones of crystals.
** Effect of weak ice melting.

Temperature of melting initiation of this phase is considered as eutectic temperature (Fig. 12a). Solubility of the halite crystals in fluid inclusions occurred at 255 to 315°C. Hence, the total salt concentration in solutions of the type III fluid inclusions is of 36 to 38 wt % $CaCl_2$ + NaCl-equiv.

In the type I and II fluid inclusions, ice melts at temperatures of –5 to –2°C (Table 4, Fig. 12b). Low eutectic temperatures ranging from –66 to –62°C and from –44 to –42°C, which are measured for these fluid inclusions, indicate a multicomponent composition of the trapped fluid. The total salt concentration estimated using ice melting temperature varies from 9.2 to 3.3 wt % NaCl-equiv (Bodnar, 1993).

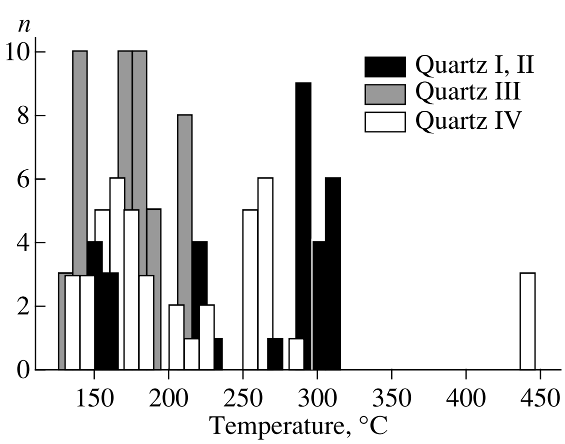

Fig. 11. Histograms for homogenization temperatures of fluid inclusions in quartz from the Kupol'noe deposit.

The ice melting temperature in fluid inclusions in quartz III and quartz IV range from –2 to –6°C and from –5 to –2°C, respectively. A weak ice melting is noticeable at heating of many fluid inclusions at –58 to –57°C. However, the intense ice melting in most of them occurs at –38 to –32°C. Thus, an increase in speed of ice melting in the liquid existing in inclusions was recorded at –38 to –32°C. These phenomena characterize the behavior of multicomponent saline solutions at low temperatures. The initial temperature of ice melting of –58 to –57°C in low concentrated solutions is close to eutectic temperatures in the water–salt systems containing $FeCl_2$ (–68 to –64°C) and $CaCl_2$ (–55 to –49.8°C). Thus, solutions contain NaCl as a dominant salt and minor $FeCl_2$ and $CaCl_2$ constituents. Salt content of 9.2 to 3.3 wt % NaCl-equiv in solutions trapped in fluid inclusions from quartz III is higher than that capsulated in fluid inclusions in quartz IV (7.9 to 3.3 wt % NaCl-equiv). Condensation of vapor phase in fluid inclusions from quartz III and IV does not even occur with their freezing to –197°C, indicating their low density.

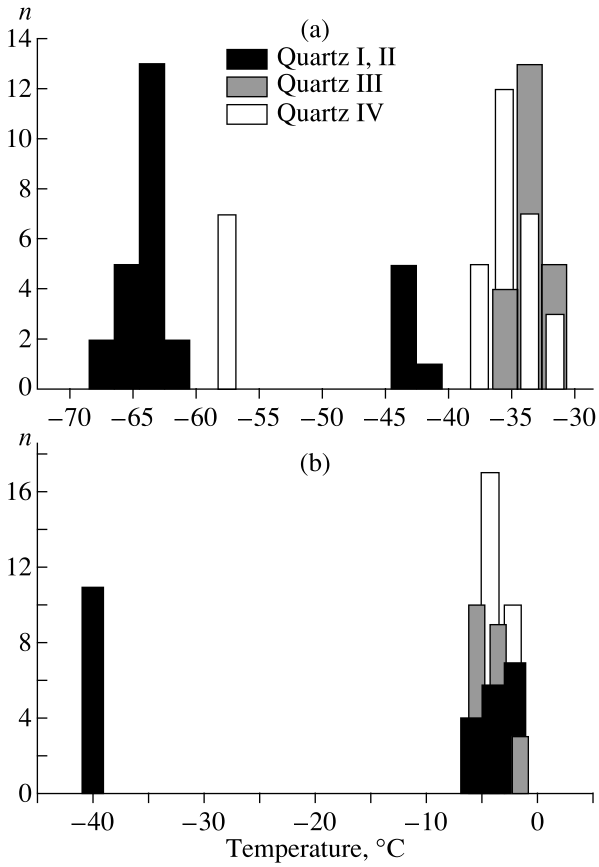

Fig. 12. Eutectic (a) and ice melting (b) temperatures in fluid inclusions in quartz from the Kupol'noe deposit (n = number of analyses).

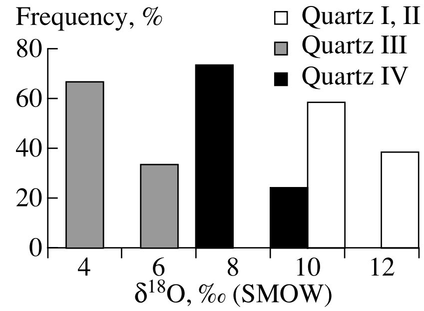

Fig. 13. Histograms for the δ^{18}O values in quartz from the Kupol'noe deposit.

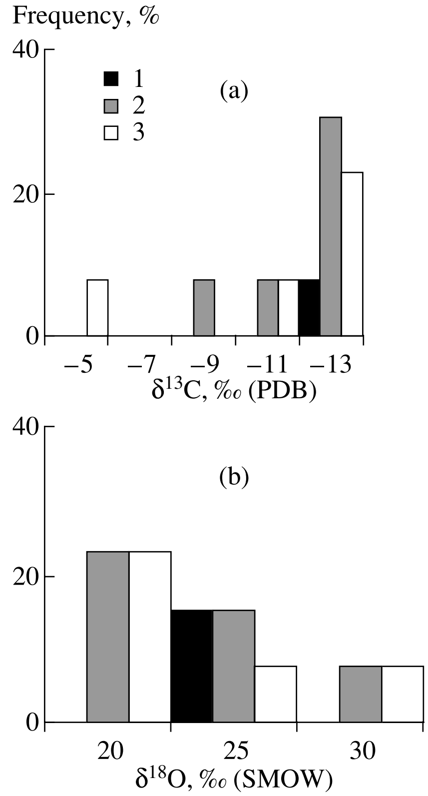

Fig. 14. Histograms for the δ^{13}C (a) and δ^{18}O (b) values for carbonates from the Kupol'noe deposit. (1) Siderite, (2) ankerite, (3) pyrite, (4) pyrrhotite.

STABLE S, O, AND C ISOTOPES

A study of stable isotopes of sulfur, carbon, and oxygen in sulfides, oxygen and carbonates was based on monomineralic separates. These separates were hand picked using a binocular microscope, and the purity of analyzed material was more than 95%. Analyses were made using standard techniques and their results are, given as δ values, refer to international standards (Kyzer, 1987).

Oxygen Isotopes in Quartz

The δ^{18}O values of quartz range from +2.3 to +11‰ (Fig. 13). The δ^{18}O values of quartz I, II, III, and IV are +6.2 to +7.9‰, +7.1 to +8.9‰, +2.3 to +5.5‰, and +8.3 to +11.0‰, respectively. The narrow ranges of isotopic composition found for each generation of quartz should be noted. Their isotopic compositions are different because the higher δ^{18}O values are characteristic of quartz IV, while the lowest values were found for quartz II.

Carbon and Oxygen Isotopes for Carbonates

The δ^{13}C values of carbonates range from –15.0 to –5.6‰ (Fig. 14a). The δ^{13}C values of different carbonates differ a little from each other, and most of them correspond to –14.4 ± 3‰, because only the two values of –9.2 and –5.6% are beyond this range. This suggests that the carbon isotopic composition did not noticeably evolve.

The δ^{18}O values of carbonates range from +17.4 to +29.2‰ (Fig. 14b). The figures obtained for siderite are +21.4 to +23.5, those of ankerite vary from +18.2 to +29.2%, and those of calcite fall between +17.4 and +26.4‰. The greatest variations are characteristic for the oxygen isotopes in minerals of the ankerite–dolo-

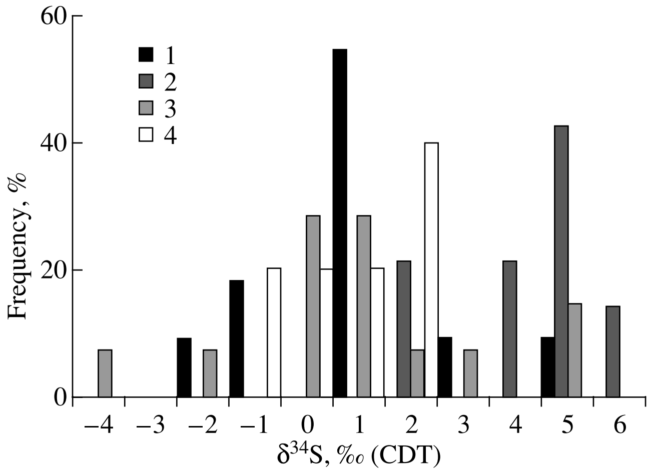

Fig. 15. Histograms for the $\delta^{34}S$ values for sulfides from the Kupol'noe deposit. (1) Galena, (2) sphalerite, (3) pyrite, (4) pyrrhotite.

mite series. The $\delta^{18}O$ values of other minerals are clustered within a narrow range.

Sulfur Isotopes in Sulfides

The isotopic compositions of pyrite, galena, and sphalerite sampled from different zones and ore bodies and pyrrhotite from granodiorite are given as histograms (Fig. 15). The $\delta^{34}S$ values of sulfides range from –4.2 to +6‰. The $\delta^{34}S$ values obtained for pyrrhotite are –1.1 to +1.8‰, those for pyrite I, II, and III are +1.5 to +4.5‰, –0.3 to +0.8‰, and –4.2 to –0.1‰, respectively, and figures obtained for galena and sphalerite range from +1.8 to +6.0% and –2.4 to +4.9‰, respectively. It can be noted that the $\delta^{34}S$ values lie in a rather narrow range. Most data points measured fall in the field of 0 ± 2%. A slight increase of $\delta^{34}S$ values for sphalerite is recorded. Possibly, this is caused by the sulfur isotope fractionation during sphalerite crystallization because a heavy sulfur isotope is preferably incorporated into its crystal structure (Ohmoto, 1972).

The most considerable variations of the sulfur isotope ratio were found in pyrite and galena. The variations of $\delta^{34}S$ values were recorded for the same generation of galena, while pyrite of different generations displayed a changing of the sulfur isotope ratio. The highest $\delta^{34}S$ values were obtained for pyrite associated with quartz I from quartz–muscovite–tourmaline metasomatic assemblage, while the lowest one is characteristic for pyrite III from the tin–silver–base metal ores. The $\delta^{34}S$ values of pyrite II associated with quartz II from the quartz–tourmaline veins which lie within an intermediate range.

Fluid Isotopic Composition

The stable isotope ratio in the mineral-forming fluid was calculated using established approaches and equations of the fractionation of stable isotopes between minerals and fluid constituents in hydrothermal systems (Field and Fifarek, 1985; Ohmoto, 1986; Sheppard, 1986). These calculations are based on the assumption that isotopic equilibrium between the crystallizing minerals and the fluid was attained and no postdepositional changes in the sulfide isotopic compositions occurred. The results of measurements of the isotopic compositions and homogenization temperatures of fluid inclusions were used for these calculations.

The oxygen isotopic composition of water that is a major constituent of the hydrothermal fluid was calculated in the quartz–water system using the following equation:

$$\Delta_{\text{quartz-H}_2\text{O}} = 1000\ln\alpha = 3.34\times(10^6/T^2) - 3.31, \quad (1)$$

where T is Kelvin temperature in this and following equations.

The homogenization temperatures of fluid inclusions in quartz I and II are from 285 to 450°C. Therefore, the $\delta^{18}O_{H_2O}$ value was calculated for 350°C and was equal to +4 ± 2‰. As a result of CO_2 separation to the vapor phase at the temperature and pressure drop, the $\delta^{18}O$ value in the residual fluid is decreased (Bowers, 1991). Apparently, the fluid can be richer in a heavy oxygen isotope before phase separation. Fluid inclusions in quartz III were homogenized at 125 to 185°C. The temperatures of their entrapment at quartz crystallization were probably higher. Hence, the $\delta^{18}O_{H_2O}$ value calculated at 200°C was equal to –8 ± 3‰. Fluid inclusions in quartz IV were homogenized at 135 to 280°C, therefore the oxygen isotopic ratio was calculated at 275°C. The values obtained fall in the field of +2 ± 2‰.

Carbon isotope composition in the hydrothermal fluid was calculated assuming that isotopic equilibrium between the fluid and minerals deposited has been attained at temperatures of 140 to 185°C, and CO_2 dissolved in the fluid was a predominant carbon species. This assumption is based on buffering the pH value at five due to the replacement reaction of K-feldspar by quartz and sericite during the formation of metasomatic wall rocks. H_2CO_3 is a predominant carbon species in such solutions. As $\delta^{13}C_{CO_2} \approx \delta^{13}C_{H_2CO_3}$ (Ohmoto, 1972), the following fractionation equations were used:

$$\Delta_{\text{siderite-CO}_2} = 1000\ln\alpha = 0.861\times10^6/T^2 + 0.82, \quad (2)$$

$$\Delta_{\text{calcite-CO}_2} = 1000\ln\alpha = 2.988\times(10^6/T^2) - 7.666\times(10^3/T) + 2.461, \quad (3)$$

$$\Delta_{\text{calcite-CO}_2} = 1000\ln\alpha = 3.168\times(10^6/T^2) - 7.666\times(10^3/T) + 2.631. \quad (4)$$

The $\delta^{13}C_{CO_2}$ of the fluid which deposited siderite was found to be –20 ± 1‰. These values can vary from –10.2 to –17.6% for fluid equilibrated with ankerite, and to be equal to –14.5‰ for the fluid in equilibrium with calcite.

Proceeding from the assumption that $\delta^{34}S_{\Sigma S} \approx \delta^{34}S_{H_2S}$, we calculated the sulfur isotopic composition in the fluid equilibrated with sulfides. The following equations of the H_2S fractionations between sulfides were used:

$$1000\ln\alpha = \delta^{34}S_{\text{pyrite}} - \delta^{34}S_{H_2S} = 0.4 \times (10^6/T^2), \quad (5)$$

$$1000\ln\alpha = \delta^{34}S_{\text{galena}} - \delta^{34}S_{H_2S} = -0.63 \times (10^6/T^2), \quad (6)$$

$$1000\ln\alpha = \delta^{34}S_{\text{sphalerite}} - \delta^{34}S_{H_2S} = 0.1 \times (10^6/T^2). \quad (7)$$

The $\delta^{34}S_{H_2S}$ value for the early fluid was calculated using the pyrite I isotopic composition. It was found that it is close to 0 ± 3‰. The sulfur isotope ratio in the fluid deposited sphalerite and galena at 125 to 185°C varied from +0.6 to +8.9‰ in equilibrium with galena and from +1.2 to +5.5‰ in equilibrium with sphalerite. The $\delta^{34}S_{H_2S}$ value of the fluid equal to about +3 ± 2‰ can be accepted. The sulfur isotope composition of the fluid which precipitated silver–antimony mineralization was calculated from the $\delta^{34}S$ values obtained for pyrite from this association. The $\delta^{34}S_{H_2S}$ values equilibrated with pyrite corresponds to – 1 ± 2‰.

FORMATION CONDITIONS OF THE DEPOSIT

Data on the textural and structural relationships among mineral aggregates, mineral composition of metasomatic wall rocks and ores, mineral chemistry, composition of fluid inclusions and stable isotope ratios in minerals allow us to constrain mineral formation conditions and composition of mineral-forming fluids, and to propose a hypothesis on sources of the fluids and their constituents responsible for the formation of the various mineralization types found in the deposit.

The formation of rare metal mineralization commenced with the greisenization of host rocks. The characteristic reaction at this alteration is a hydrolysis of K–feldspar and its replacement for the quartz–sericite aggregate:

$$\begin{aligned} &3KAlSi_3O_8(\text{K-feldspar}) + 2H^+ \\ &= KAl_3Si_3O_{10}(OH)_2(\text{sericite}) \\ &\quad + 6SiO_2(\text{quartz}) + 2K^+. \end{aligned} \quad (8)$$

The reaction occurs with a proton consumption that indicates the neutralization of the acid fluid at its interaction with the host rocks. Rafal'skii (1987) calculated that the pH value of a solution equilibrated with this assemblage at 400°C, pressure of 1 kbar, and a 1 molar total concentration is of 4.1. This assumes that the initial mineral-forming fluid had low pH.

The deposition of wolframite and arsenopyrite can be described by the following reactions:

$$H_2WO_4^0 + FeCl_2^0 = FeWO_4(\text{wolframite}) + 2HCl^0, \quad (9)$$

$$\begin{aligned} &4FeCl_2^0 + 4H_2S^0 + 4H_3AsO_3^0 \\ &= 4FeAsS(\text{arsenopyrite}) + 2O_2 + 4HCl^0 + 8H_2O. \end{aligned} \quad (10)$$

A release of H^+ or HCl^0 occurs at the wolframite crystallization, but the temperature drop plays a more significant role (Heinrich, 1990). Reaction (10), describing the congruent solubility of arsenopyrite, depends mainly on oxygen activity rather than temperature (Heinrich and Eadington, 1986). Decrease of oxygen activity stimulates the crystallization of arsenopyrite. Both reactions result in the interaction of metal transported by the fluid and iron released from host rocks. Taking into account a low grade of both these minerals in the altered rocks, the mixing of the fluid, filtered through rocks with the earlier fluid equilibrated with this rock during its replacement at the boundary between different metasomatic zones, can be assumed to have resulted in the crystallization of wolframite and arsenopyrite.

The crystallization of the arsenopyrite–cassiterite assemblage can occur due to the following reaction:

$$\begin{aligned} &3SnCl_2^0 + 2H_3AsO_3^0 + 2FeCl_2^0 + 2H_2S^0 \\ &= 3SnO_2(\text{cassiterite}) + 4FeAsS(\text{arsenopyrite}) \\ &\quad + 2O_2 + 4HCl^\circ + 8H_2O, \end{aligned} \quad (11)$$

if redox–oxidation conditions are controlled by the reactions between component migrating in the fluid (Heinrich and Eadington, 1986). The thermodynamic simulations made by these authors have shown that the deposition of cassiterite may be described by the following reaction:

$$\begin{aligned} &SnCl_2^0 + H_2O + 0.5O_2 \\ &= SnO_2(\text{cassiterite}) + 2H^+ + Cl^-, \end{aligned} \quad (12)$$

which is caused by the reduction of the mineral-forming fluid. The reaction of the arsenopyrite crystallization can be a result of this reduction. Temperatures between 320 and 400°C and f_{O_2} equal to 10^{-30} to 10^{-35} bars are the most favorable conditions for the cassiterite deposition.

The rare metal mineralization was deposited in the mineral-forming system where two fluids simultaneously circulated. One of them was a high-concentrated (36–38 wt % NaCl +$CaCl_2$-equiv) aqueous brine, which contained predominantly NaCl and minor $CaCl_2$ and $FeCl_2$ amounts. The second fluid was vapor-rich. The vapor phase consisted of CO_2 and CH_4. The liquid phase was a dilute fluid with the salinity of 3.3 to 4.9 wt % NaCl-equiv. The mineral crystallization occurred at 285 to 450°C as the homogenization temperature of fluid inclusions may be considered as true mineral formation temperatures. The presence in zoned crystals of quartz of fluid inclusions homogenized at lower temperatures suggests that temperature and the concentration of the mineral-forming solutions decreased during mineral formation of the tourmaline–cassiterite–quartz assemblage. A source of these fluids cannot be unambiguously identified based on the oxygen isotope ratio in water. The $\delta^{18}O$ values of +4 ± 2‰ are lower than those of the +5.5 to +9.5‰ ascribed to typical magmatic water. The chemical and isotopic compositions of the fluids are mainly identical to those responsible for the formation of tin deposits (Heinrich *et al.*, 1989). Its depletion in the heavy isotope relative to a magmatic fluid possibly resulted from the following processes: (1) the fluid/rock interaction; (2) the phase separation of the fluid, or (3) the involvement of the isotopically light meteoric water in the mineral-forming systems. The study of fluid inclusions has shown that the last two phenomena occurred at the crystallization of quartz I and II. The covariant temperature and fluid salinity decreasing indicates the mixing of the high-concentrated fluid with diluted cold water of meteoric origin (Roedder, 1984).

Brines may be formed during evolution of a fluid exsolved from granite magma at its crystallization. In this case, the separation of single-phase supercritical fluid with moderate salt concentration (~8 wt % NaCl-equiv), or the liquid saline aqueous phase with high density and the vapor low saline phase occurs (Burnham, 1979; Fournier, 1987). The vapor phase with low salt content and high-concentrated fluid (up to 55 wt % NaCl-equiv) is formed at the phase separation of the low-saline fluid (Henley and McNabb, 1978; Sinohara and Hedenquist, 1997).

The sulfur isotope ratio of 0 ± 3‰ in the fluid which deposited the rare metal ores corresponds to the $\delta^{34}S$ values typical for mantle or magmatic sulfur (Ohmoto, 1986).

The above consideration suggests that the fluid related to the granite magmatism was involved in the formation of the rare metal ores. Possibly, at the ore formation site, it was mixed with the fluid formed due to the evolution of meteoric water. Sulfur could be directly introduced from a magmatic chamber or leached from host magmatic rocks.

The formation of the tin–silver–base metal mineralization and the adjacent quartz–sericite wall rocks occurred after the intense brecciation of the products of the first megastage. The later crystallization of the cassiterite–arsenopyrite–quartz mineral aggregates relative to the carbonate–sulfide ore indicates a drastic change in the mineral-forming conditions. The rare quartz III tiny veinlets and the manganosiderite fragments in the carbonate aggregates testify to the intraore cataclasis. Further on, the cassiterite–arsenopyrite–quartz assemblage was changed by the chalcopyrite–sphalerite–galena–quartz one, and then by galena–freibergite–pyrargyrite, galena–hocartite–franckeite, and the latest marcasite–ankerite assemblage. A rhythmical opening of fractures, inflowing of the compositionally variable fluids, and changing in mineral crystallization conditions are typical features of the carbonate–base metal mineralization.

The formation temperature of quartz–sericite rocks and the $\log(a_{K^+}/a_{H^+})$ ratio in the hydrothermal fluid were estimated using the composition of sericite coexisting with different minerals. The T°C vs. $\log(a_{K^+}/a_{H^+})$ plot of the satiability fields for quartz-bearing assemblages, mica, and chlorite with the Al^{IV} isopleths was used for this purpose (Kol'tsov, 1992). We assume that a monovariant reaction of the replacement of K-feldspar for quartz and muscovite was characteristic for formation conditions of the quartz–sericite wall rocks. The association of K–feldspar, sericite containing 0.76 atoms of Al^{IV} per formula, and quartz in these rocks could be formed in outer zone at 275 to 290°C and an $\log(a_{K^+}/a_{H^+})$ value of 4.65 to 4.8 in the hydrothermal fluid. The intermediate zone, where sericite contains 0.81 to 0.82 atoms of Al^{IV} per formula, was formed at 290 to 305°C and an $\log(a_{K^+}/a_{H^+})$ value of 4.55 to 4.65. Minerals from the inner feldspar-free zone, where sericite contains 0.84 atoms of Al^{IV} per formula crystallized below 285 to 350°C at the $\log(a_{K^+}/a_{H^+})$ value of 4.5 to 4.6 in the hydrothermal solution. Thus, the formation of the quartz–sericite wall rocks occurred at 275 to 350°C at an interaction of host rocks, and the hydrothermal fluid had an $\log(a_{K^+}/a_{H^+})$ ratio of 4.5 to 4.8. The temperature and acidity of the mineral-forming fluid were decreased from the inner to outer zone in the alteration halo.

Quartz from the carbonate-quartz–sulfide veins was deposited from low-temperature solutions. The homogenization temperatures of fluid inclusions in this mineral are 125 to 185°C. These values may be considered as the minimal temperatures of the quartz deposition, as the estimation of true mineral formation temperature requires a pressure correction of the measured values (Roedder, 1984). The homogenization temperatures of fluid inclusions which trapped the "boiling" fluid may be considered as true temperatures. No direct evidence for quartz deposition resulting from the "boiling" fluid, nor the coexisting vapor-rich and liquid-rich fluid inclusions, has been recorded. However, we suppose that fluid boiling played an important role in the formation of the quartz–carbonate–sulfide veins. The escape of gaseous CO_2 from the fluid led to the voluminous deposition of carbonates due to a temperature drop from 280 to 245°C and a pH increase (Reed and Spycher, 1985). Other phenomena such as the temperature and pH decrease at the conductive cooling of the fluid are not the effective mechanisms in the carbonate precipitation. An occurrence of cavities in the carbonate aggregates filled in by later minerals evidence fluid boiling. These cavities are inferred to have trapped gaseous bubbles responsible for the crystallization of the late minerals. It may be supposed that the escaped CO_2 was incorporated into deposited carbonates. Fluid inclusions in quartz could predominantly entrap the aqueous phase due to different wettability (Alekhin, 1985).

Fabrics of the carbonate–quartz–sulfide veins are similar to the rhythmically banded veins in epithermal deposits of precious metals. Their formation is accompanied by multiple reopening of fractures resulting in fluid "boiling" and a volatile escape, mainly of CO_2. This phenomenon caused the mineral deposition and fracture sealing. New fluid pulses ascending from the abyssal zones of a hydrothermal system to a near-surface environment "boiled" again due to the fluid overpressure on the lithostatic load of host rocks (Hedenquist and Henley, 1985; Fournier, 1987; Henley and Hughes, 2000). This resulted in the fracture formation and cataclasis of previously deposited minerals.

The concentration of dissolved salts in the fluid was from low to moderate (3.3 to 9.2 wt % NaCl-equiv). NaCl was predominant among them, while $CaCl_2$ and $FeCl_2$ were subordinate species.

The oxygen isotope ratio in this fluid ($\delta^{18}O = -8 \pm 2‰$) suggests that a heated meteoric water was its important constituent. Carbon in the fluid was considerably depleted in the $\delta^{13}C$ isotope ($\delta^{13}C = -14$ to $-20‰$). The chromatographic gas analysis has shown the presence of methane in the gaseous phases in fluid inclusions. However, rather high methane content in the fluid is required to provide a sufficient isotopic shift. Such $\delta^{13}C$ values may indicate an involvement of organic carbon in the ore formation ($\delta^{13}C_C$ up to $-30‰$) (Field and Fifarek, 1985). It could be leached from granite enclosing graphite segregations and from terrigenous rocks containing the carbonaceous matter. Therefore, the carbon isotope shift to the ^{13}C isotope depletion may be caused by the presence of isotopically light methane and carbon incorporated by fluid at its interaction with these rocks. The sulfur isotope ratio ($\delta^{34}S_{H_2S} = -1 \pm 2‰$) is typical for magmatic or mantle sulfur. The data obtained indicate that the mineral-forming fluid which deposited the silver–base metal ores was a heated meteoric water bearing methane and carbon dioxide leached from magmatic and sedimentary rocks. Sulfur hydrogen possibly derived from magmatic host rocks as well.

The intense cataclasis and fracturing of the mineral aggregates of early mineralization types preceded the formation of the silver–antimony mineralization. The mineral-forming process initiated from the argillization of host rocks. This process occurred most intensely at the overprinting onto the carbonate-bearing facies of quartz–sericite rocks because their minerals were unstable under these conditions.

The stability of argillized rocks is controlled by the following reaction:

$$2KAl_2(AlSi_3O_{10})(OH)_2 + 3H_2O + 2H^+ = 3Al_2Si_2O_5(OH)_4 + 2K^+. \quad (13)$$

The pH value was <3 at 250°C and the K^+ molality of 1 that resulted in the acid alteration of host rocks, leaching of SiO_2 from feldspars and other silicates, and its dissolution in the fluid that became oversaturated relative to quartz and amorphous silica (Fournier, 1985). The fluid neutralization at its boiling and the CO_2 escape caused the silica precipitation.

Textural–structural features of quartz veins indicate that they were formed from the fluid oversaturated with quartz and, possibly, with amorphous silica. This conclusion follows from colloform and concentrically zoned quartz indicating the existence of numerous crystallization centers. Such fabrics are typical for epithermal deposits. Saturation with fluid and mineral inclusions of quartz corresponds to periods of fluid boiling that in conjunction with the textural features suggest a shallow ore deposition. Carbon dioxide, heavy carbonaceous gaseous species in vapor phase and aqueous phases were detected in fluid inclusions.

The precipitation of silver–antimony ores started at higher temperatures than the deposition of earlier silver–base metal ores. Homogenization temperatures of fluid inclusions in quartz range from 135 to 280°C. The concentration of dissolved salts in the fluid is slightly lower (7.9 to 3.3 wt % NaCl-equiv). The presence of jarosite indicates that the mineral formation occurred under high oxidation potential. Marcasite and pyrite were deposited at a temperature below 240°C from acid solutions with the pH value <5 (Murowchick and Barnes, 1986). A prerequisite for the marcasite formation is the oxidation of sulfur hydrogen to polysulfide species like H_2S_n. The marcasite occurrence in the quartz–antimony ores shows that their crystallization temperature was below 240–250°C and pH < 5. This also indicates ore deposition in a shallow environment.

The oxygen isotope ratio in this fluid ($\delta^{18}O = +2 \pm 2‰$) suggests a considerable fraction of heated evolved meteoric waters in the fluid. Nevertheless, this fluid is richer in ^{18}O isotope relative to the fluid which deposited the silver–base metal ores. The sulfur isotope ratio ($\delta^{34}S_{H_2S} = +3 \pm 2‰$) indicates its magmatic origin. The fluid, which was enriched by 3–4‰ in the ^{34}S isotope in comparison with the hydrothermal solution, deposited the silver–base metal ores.

MODEL FOR THE DEPOSIT FORMATION

The above data allow us to suggest the hypothesis that the genetically diverse ores have been formed at different depths and under different physical conditions, and that the compositionally different fluids derived from various sources and were involved in the ore-forming system. The main question is whether the ore mineralization originated during successive stages of a single mineral-forming process and indicates an evolution of the fluid regime in the hydrothermal system related to emplacement of a magma chamber, or each mineralization type is associated with a separate geological process. This problem was previously considered with reference to cassiterite deposits. Several researches suggested that during the formation of mesothermal tin deposits, the mineral-forming fluid evolved spatially and temporally from a lithostatic pressure environment to the low temperature ore deposition at hydrostatic pressure (Heinrich *et al.*, 1989). The mineral-forming fluid which deposited the cassiterite ores exsolved from a magma chamber at lithostatic pressure, and then interacted with meteoric water and cooled at shallow depths.

The diverse mineralization types at the Kupol'noe deposit are confined to the different fault and fracture systems. Each of them is characterized by a definite combination of the mineral assemblages and is accompanied by the alteration halo intrinsic to this mineralization only. The rare metal mineralization formed under abyssal and high-temperature conditions from the high-mineralized fluid. It is known that in quartz from tin deposits, fluid inclusions were trapped at pressures of 300 ± 100 bars (Heinrich *et al.*, 1989). The formation depth of such ores was about 1 km at lithostatic pressure. The silver–base metal and silver–antimony deposits formed under shallow and mid-temperature conditions with a considerable involvement of the meteoric water in the ore formation. If the hypothesis on boiling of the fluid is true, the depositional depth of minerals at hydrostatic pressure from the fluid with a salinity of 3 to 9 wt % NaCl-equiv at 225–250°C should be about 300–400 m (Henley *et al.*, 1984). This allows us to suppose that the different mineralization types at the Kupol'noe deposit were formed at different megastages of the geological district development, separated by the period when the rare metal mineralization was uplifted to a more shallow depth. The silver–base mineralization was deposited in a near-surface environment. The silver–antimony mineralization was formed at a depth of 300 m. This is evidenced for the formation of hypogenous jarosite (Harvey and Vitaliano, 1964). The tin–silver–base metal mineralization underwent the hypergenous alteration between the formation of tin–silver–base metal and silver–antimony mineralizations. The fragments of the former were capsulated in the mineral aggregates of the silver–antimony type.

In our opinion, the rare metal (tin–tungsten), tin–silver–base metal, and silver–antimony mineralization types are related to the different megastages of the geodynamic development of the Verkhoyansk–Kolyma fold belt. It should be remembered that only a single type of mineralization has been recorded at most of deposits in this territory. At each deposit, a mineralization is accompanied by a similar alteration halo and their mineral aggregates have been formed according to the sequence established at the Kupol'noe deposit. In the Verkhoyansk–Kolyma fold belt, the rare metal, tin–silver–base metal, and silver–antimony deposits are linked with the magmatic associations dated by the ^{40}Ar-^{39}Ar technique (Parvenov *et al.*, 1999). It was established that the cassiterite ores are associated with the granodiorite magmatic complexes emplaced between 120 and 134 Ma ago. The silver–base–metal and silver–antimony deposits formed after the intrusion of silicic subvolcanic dikes dated at 80 to 100 Ma.

The setting of the Kupol'noe deposit in an extremely active area of the Verkhoyansk–Kolyma belt confined to a convergence of three large plates which have played an important role in its development (Fujita *et al.*, 1997). This predetermined the diverse magmatism related to the different megastages in the geodynamic history of this region. The Kupol'noe ore–magmatic system originated at the postcollision period after the emplacement of the collision granites and the intrusion of dacites of the Taryn subvolcanic massif at 124 to 144 Ma ago. An intermediate magmatic chamber was formed at the activation of the Adycha–Taryn fault and the rejuvenation of the submeridional abyssal fault. The depth of this magmatic chamber is estimated as 7–8 km with the help of geophysical data and from the composition of rock-forming garnet (Stognii *et al.*, 2000). The derivates of this chamber are rocks of the Trud and Kapriznyi massifs intruded at 125 Ma. The similarity of accessory mineralization (tourmaline and cassiterite) in these granitoids and trace elements chemistry of accessory and metasomatic tourmaline, cassiterite, pyrite, and arsenopyrite evidence the genetic affinity of the rare metal mineralization and these magmatic rocks.

The next megastage in the development of the Kupol'noe ore–magmatic system was linked with the initiation of the Okhotsk subduction in the Late Cretaceous. At first, the granodiorite-porphyry dikes, dated at 100 Ma, were intruded (Nenashev and Zaitsev, 1980). They intersect the Early Cretaceous massifs outcropping around the Taryn subvolcano. These dikes are similar in many respects with rocks of this intrusive complex. They contain garnet and graphite as well. However, their relationships to the ore mineralization have not been established. It remains unclear whether their age corresponds to the tectonomagmatic activation period (Bakharev *et al.*, 1997). It is not excluded that the injection of granite-porphyry dikes, resulted in the creation of a convective cell and the activization of the shallow hydrothermal system, where meteoric waters predominated. This led to the formation of the tin–silver–base metal ores. Geodynamic reconstructions indicate opening of northeastern fractures in the extension environment (Parfenov *et al.*, 2001). This favored the deposition of the tin–silver–base metal mineralization in the diagonal fracture system.

The formation of the silver–antimony mineralization was possibly related to the postsubduction activization of long-lived faults in the Verkhoyansk–Kolyma belt in the Late Cretaceous. The continental silicic subvolcanic magmatism and related epithermal gold–silver and silver–antimony ore mineralization were formed during this period. This activization affected the Adycha–Taryn fault zone and resulted in the formation of the silver–antimony ore mineralization at the Kupol'noe deposit. The latter occurs in the sublatitudinal fractures in the Taryn subvolcano without any links with the rare metal and base metal ores. The K–Ar age of the adularia wall rocks enclosing the silver–antimony ore mineralization is 73 Ma (Nenashev and Zaitsev, 1980).

Thus, the ore mineralizations at the Kupol'noe deposit were formed during three megastages. The first two megastages (rare metal and tin–silver–base metal) are characterized by tin specialization and are intimately related to the collision and development of the Kupol'noe granite-related ore–magmatic system. They are spatially associated, though they are controlled by different fractures. Physical and chemical conditions of mineral-forming processes in them are substantially different. The silver–antimony megastage of ore formation is linked with the postcollision activization and the activity of shallow fluid systems.

CONCLUSION

The investigations carried out indicate that a transition from the mesoabyssal high-temperature (mesothermal) ore–magmatic system, in which high-concentrated magmatic fluid predominated, to the shallow middle–low-temperature hydrothermal system where low saline fluids which modified meteoric waters prevailed, has occurred during the formation of the Kupol'noe deposit. The fluid regime in the Kupol'noe hydrothermal system was different from that previously suggested for the Prognoz ore forming system in which mineral aggregates of different ages were formed under similar physical and chemical conditions at relatively low temperatures (100 to 250°C) from reduced aqueous–methane–nitrogen–carbon dioxide moderate-concentrated (8.0 to 29.0 wt % NaCl + $CaCl_2$-equiv) chlorine solutions (Gamyanin *et al.*, 1998). It was assumed that the concentration of dissolved salts and gaseous components in the fluid and its isotopic composition did not radically change. The Prognoz deposit most likely formed as a result of the activity of the long-lived ore-forming hydrothermal system linked with a single reservoir or similar reservoirs, while different ore–magmatic systems were responsible for the formation of the Kupol'noe deposit.

ACKNOWLEDGMENTS

This study was supported by the Russian Foundation for Basic Research (projects 98-05-65264 and 00-05-65077).

REFERENCES

Alekhin, Yu.V., On Different Representativeness of Gas–Liquid Inclusions in Relation to Parameters of the Mineral Formation Medium, *Tez. dokl. VII Vsesoyuz. soveshch. "Termobarometriya i geokhimiya rudoobrazuyushchikh flyuidov"* (VII All-Union Conference on Thermobarometry and Geochemistry of Ore-Forming Fluids), L'vov: L'vovskii Gos. Univ., 1985, part 1, pp. 6–8.

Bakharev, A.G., Zaitsev, A.I., Nenashev, N.I., *et al.*, The Structure and Magmatism of Verkhne-Indigirskaya Ring Structure, *Otech. Geol.*, 1997, no. 9, pp. 15–19.

Bodnar, R.J., Revised Equation and Table for Determining the Freezing Point Depressions of H_2O–NaCl Solutions, *Geochim. Cosmochim. Acta*, 1993, vol. 57, pp. 688–684.

Bodnar, R.J., Reynolds, T.J., and Kuehn, C.A., Fluid Inclusion Systematics in Epithermal Systems, *Geology and Geochemistry of Epithermal Systems*, El Pasco: Econ. Geol., 1984, pp. 73–97.

Borisenko, A.S., The Study of Salt Composition of Solutions from Gas–Liquid Inclusions in Minerals by Cryometry, *Geol. Geofiz.*, 1977, no. 8, pp. 16–28.

Borisenko, A.S., Borovikov, A.A., Pavlova, G.G., and Mortsev, N.K., Physicochemical Conditions of Formation of Silver–Antimony Mineralization in the Bazardarin Ore Field, *Granitoidnyi magmatizm i orudenenie Bazardarinskogo gornorudnogo raiona (Yuzhnyi Pamir)* (Granitoid Magmatism and Mineralization of Bazardarin Ore-Mining District), Novosibirsk: IGiG, 1990, pp. 160–180.

Borisenko, A.S., Kolmogorov, A.I., Borovikov, A.A., Shebanin, A.P., and Babich, V.V., Composition and Metal-bearing Potentials of Ore-Forming Solutions in the Deputat Tin-Ore Deposit (Yakutia), *Geol. Geofiz.*, 1997, vol. 38, no. 11, pp. 1830–1871.

Borovikov, A.A., Physicochemical Conditions and Main Factors of Formation of Silver–Antimony and Tin–Tungsten Ore Mineralization in Bazardarin Ore Field (Southeastern Pamirs), *Extended Abstracts of Cand. Sci. (Geol.–Miner.) Dissertation*, Novosibirsk, 1995.

Bortnikov, N.S., On the Reliability of the Arsenopyrite and Arsenopyrite–Sphalerite Geothermometers, *Geol. Rudn. Mestorozhd.*, 1993, vol. 35, no. 2, pp. 177–191.

Bortnikov, N.S., Nekrasov, I.Ya., and Mozgova, N.N., Phase Interrelations in Ternary Sections of the Fe–Pb–Ag–Sb–As–S System and Their Implication for the Sulfosalt Mineralogy, *Sul'fosoli, platinovye mineraly i rudnaya mikroskopiya* (Sulfosalts, Platinum Minerals, and Ore Microscopy), Moscow: Nauka, 1980, pp. 66–74.

Bortnikov, N.S., Gamyanin, G.N., Alpatov, V.V., *et al.*, Mineralogical and Geochemical Features and Formation Conditions of Nezhdaninskoe Gold Deposit (Sakha-Yakutia, Russia), *Geol. Rudn. Mestorozhd.*, 1998, vol. 40, no. 2, pp. 137–156.

Bowers, T.S., The Deposition of Gold and Other Metals; Pressure-Induced Fluid Immiscibility and Associated Stable Isotope Signatures, *Geochim. Cosmochim. Acta*, 1991, vol. 55, pp. 2417–2434.

Burnham, C.W., *Magmas and Hydrothermal Fluids. Geochemistry of Hydrothermal Ore Deposit*, New York: Wiley, 1979, pp. 71–136.

Ermakov, N.P., *Geokhimicheskie sistemy vklyuchenii v mineralakh* (Geochemical Systems of Inclusions in Minerals), Moscow: Nedra, 1972.

Ermolov, P.V., Izokh, A.E., and Vladimirov, A.G., Garnet As an Indicator of Granite Formation Conditions in the Crust, *Dokl. Akad. Nauk SSSR*, 1979, vol. 246, no. 1, pp. 208–211.

Field, C.W. and Fifarek, R.N., Light Stable Isotope Systematics in the Epithermal Environment, *Geology and Geochemistry of Epithermal Systems*, El Pasco: Econ. Geol., 1985, pp. 99–128.

Flerov, B.L., *Olovorudnye mestorozhdeniya Yano-Kolymskoi skladchatoi oblasti* (Tin–Ore Deposits of Yana–Kolyma Fold Region), Novosibirsk: Nauka, 1976.

Fournier, R.O., Conceptual Models of Brine Evolution of Magmatic–Hydrothermal Systems, *US Geol. Surv. Prof. Paper*, 1987, vol. 1350, pp. 1487–1506.

Fournier, R.O., The Behavior of Silica in Hydrothermal Solutions, *Geology and Geochemistry of Epithermal Deposits (Systems)*. El Pasco: Econ. Geol., 1985, pp. 45–62.

Fujita, K., Stone, D.V., Layer, P.W., Parfenov, L.M., and Kozmin, B.M., Cooperative Program Helps Decipher Tectonics of Northeastern Russia, *Am. Geophys. Union*, 1997, vol. 78, no. 24, pp. 245–253.

Gamyanin, G.N., Anikina, E.Yu., Bortnikov, N.S., *et al.*, The Prognoz Silver–Polymetallic Deposit, Yakutia: Mineralogy, Geochemistry, and Origin, *Geol. Rudn. Mestorozhd.*, 1998, vol. 40, no. 5, pp. 440–458.

Harvey, R.D. and Vitaliano, C.Y., Wall-Rock Alteration in the Goldfield District, Nevada, *J. Geol.*, 1964, vol. 2, no. 5.

Hedenquist, J.W. and Henley, R.W., The Importance of CO_2 on Freezing Point Measurements of Fluid Inclusions: Evidence from Active Geothermal Systems and Implications for Epithermal Ore Deposition, *Econ. Geol.,* 1985, vol. 80, pp. 1379–1406.

Heinrich, C.A., The Chemistry of Hydrothermal Tin (–Tungsten) Ore Deposition, *Econ. Geol.*, 1990, vol. 85, pp. 457–481.

Heinrich, C.A. and Eadington, P.J., Thermodynamic Predictions of the Hydrothermal Chemistry of Arsenic, and Their Significance for the Paragenetic Sequence of Some Cassiterite–Arsenopyrite–Base Metal Sulfide Deposits, *Econ. Geol.*, 1986, vol. 81, pp. 511–529.

Heinrich, C.A., Henley, R.W., and Seward, T.M., *Hydrothermal Systems*, Adelaide: Australian Mineral Foundation, 1989.

Henley, R.W. and Hughes, G.O., Underground Fumaroles: "Excess Heat" Effects in Vein Formation, *Econ. Geol.*, vol. 95, pp. 453–467.

Henley, R.W. and McNabb, A., Magmatic Vapor Plumes and Ground Water Interactions in Porphyry Copper Emplacement, *Econ. Geol.*, 1978, vol. 73, pp. 1–20.

Henley, R.W., Trusdell, A.H., and Barton, P.V., *Fluid Mineral Equilibria in Hydrothermal Systems*, El Pasco: Econ. Geol., 1984.

Kol'tsov, A.B., Formation Conditions of Micas and Chlorites of Variable Composition in Metasomatic Processes, *Geokhimiya*, 1992, no. 6, pp. 846–857.

Kosovets, T.N., Karpinskii, N.I., Zarudnyi, N.N., *et al.*, Volcanogenic Silver Mineralization in Orogenic Structure of Mesozoides, *Rudonosnye geologicheskie formatsii* (Ore-bearing Geological Formations), Moscow: TsNIGRI, 1984, pp. 45–52.

Kotlyar, I.N., Zhulanova, N.L., Rusakov, T.B., and Gagieva, A.M., Scheme of Subdivision of Mesozoic Magmatic Complexes in Kolyma–Okhotsk Region and Some Features of Their Evolution, *Petrografiya na rubezhe XXI veka* (Petrography on the Boundary of XXI Century), Syktyvkar: Inst. Geol. Komi Nauchn. Tsentr Ross. Akad. Nauk, 2000, vol. 1, pp. 273–276.

Kyzer, T.K., *Stable Isotope Geochemistry of Low Temperature Fluids*, Saskatoon: Mineral. Association of Canada, 1987.

Layer, P.W., Newberry, R., Fujita, K., Parfenov, L.M., Trunilina, V., and Bakharev, A., Tectonic Setting of and Plutonic Belts of Yakutia, Northeast Russia, Based on $^{40}Ar/^{39}Ar$ Geochronology and Trace Element Geochemistry, *Geology*, vol. 29, pp. 167–170.

Makovicky, E. and Karup-Møller, S., Chemistry and Crystallography of Lillianite Homologous Series. Part I: General Properties and Definitions, *Neues Jahrbuch fur Mineralogie. Abh.*, 1977, pp. 264–287.

Moelo, Y., Mozgova, N.N., Picot, P., Bortnikov, N.S., and Vrublevskaya, Z., Cristallochimie de l'owyheeite: nouvelles donnees, *Tschermaks. Mineralogische und Petrograhische Mitteilungen*, 1984, vol. 2, pp. 271–284.

Mozgova, N.N., Nenasheva, S.N., Borodaev, Yu.S., *et al.*, New Data on Antimony–Bismuth Sulfosalts As a Possible Source of Additional Minerals on Sn–W Deposits, *Dokl. Sov. Geol. Mineralogiya* (Reports of the Soviet Geologists), Moscow: Nauka, 1989, pp. 197–204.

Murowchick, J.B. and Barnes, H.L., Marcasite Precipitation from Hydrothermal Solutions, *Geochim. Cosmochim. Acta*, 1986, vol. 50, no. 12, pp. 2615–2629.

Naiborodin, V.I., Sidorov, A.A., and Tolstikhin, Yu.V., On Formational Independence of Tin–Silver Deposits, *Dokl. Akad. Nauk SSSR*, 1974, vol. 218, no. 2, pp. 430–433.

Nedosekin, Yu.D. and Shkodzinskii, V.S., *Granitoidy glavnogo batolitovogo poyasa, ikh tipizatsiya i geokhimicheskie usloviya formirovaniya (Vostochnaya Yakutiya)* (Granitoids of the Main Batholithic Belt and Their Typization and Geochemical Environment of Formation, Eastern Yakutia), Yakutsk: Nauka, 1991.

Nekrasov, I.Ya., Troneva, N.V., Chevychelov, V.Yu., and Gamyanin, G.N., Parageneses of Okartite from the Pereval'noe Deposit, *Dokl. Akad. Nauk SSSR*, 1978, vol. 239, no. 3, pp. 90–95.

Nekrasova, A.N. and Demin, G.P., On Interrelation between Gold–Silver and Tin–Silver Mineralizations on a Volcanic Deposit, *Geol. Rudn. Mestorozhd.*, 1977, no. 1, pp. 105–108.

Nenashev, N.I., *Magmatizm i razvitie rudno-magmaticheskikh uzlov Vostochnoi Yakutii* (Magmatism and Evolution of Ore-Magmatic Groups in Eastern Yakutia), Novosibirsk: Nauka, 1979.

Nenashev, N.I. and Zaitsev, A.I., *Geokhronologiya i problemy genezisa granitoidov Vostochnoi Yakutii* (Geochronology and Problems of the Genesis of Granitoids in Eastern Yakutia), Novosibirsk: Nauka, 1980.

Ohmoto, H., Systematics of Sulfur and Carbon Isotopes in Hydrothermal Ore Deposits, *Econ. Geol.*, 1972, vol. 67, pp. 551–578.

Ohmoto, H., Stable Isotope Geochemistry of Ore Deposits, *Review in Mineralogy*, 1986, vol. 16, pp. 491–560.

Parfenov, L.M., Terranes and the History of Formation of Mesozoic Orogenic Belts in Eastern Yakutia, *Tikhookean. Geol.*, 1995, vol. 14, no. 6, pp. 32–43.

Parfenov, L.M., Nokleberg, U.J., Monger, J.N., *et al.*, Formation of Collage of Terranes in Orogenic Belts of the Northern

Pacific Frame, *Geol. Geofiz.*, 1999, vol. 40, no. 11, pp. 1563–1574.

Parfenov, L.M., Trunilina, N.V., Gamyanin, G.N., and Yakovlev, Ya.V., Geodynamic, Magmatism, and Metallogeny of the Verkhoyansk–Kolyma Mesozoides, *Zakonomernosti razmeshcheniya poleznykh iskopaemykh (Metallogeniya Sibiri)* (Distribution Patterns of Mineral Resources—Metallogeny of Siberia), Moscow: Nauka, 1988, vol. 15, pp. 179–188.

Popov, L.N. and Kuznetsov, Yu.V., Age of Magmatic Complexes of the Sarychev Ridge, *Sov. Geol.*, 1987, no. 12, pp. 91–96.

Rafal'skii, R.P., To the Problem of Acidity of Hydrothermal Solutions, *Geokhimiya*, 1987, no. 2, pp. 402–415.

Reed, M.H. and Spycher, N.F., Boiling, Cooling and Oxidation in Epithermal Systems: a Numerical Modeling Approach, *Geology and Geochemistry of Epithermal Systems*, El Pasco: Econ. Geol., 1985, pp. 249–272.

Roedder, E., Fluid Inclusions, *Review in Mineralogy*, 1984, vol. 12.

Rudich, K.N., *Magmatizm khrebta Sarycheva* (Magmatism of the Sarychev Ridge), Moscow: Gostekhizdat, 1959.

Sheppard, S.M.F., Characterization and Isotopic Variations in Natural Waters, *Rev. Mineral.*, 1986, vol. 16, pp. 165–183.

Shkodzinskii, V.S., Nedosekin, Yu.D., and Surnin, A.A., *Petrologiya pozdnemezozoiskikh magmaticheskikh porod Vostochnoi Yakutii* (Petrology of the Late Mesozoic Magmatic Rocks of Eastern Yakutia), Novosibirsk: Nauka, 1992.

Sinohara, H. and Hedenquist, J.W., Constraints on Magma Degassing Beneath the Far Southeast Porphyry Cu–Au-Deposit, Philippines, *J. Petrol.,* 1997, vol. 38, pp. 1741–1752.

Stognii, V.V., Stognii, G.A., and Vasil'ev, S.P., Gravity and Magnetic Fields in Yakutia, *Geofizika*, 2000, no. 2, pp. 48–51.

Stognii, G.A., Stognii, V.V., Vasil'ev, S.P., and Chernikov, V.I., Geophysical Fields in Yakutia As Indicators of Geodynamic Conditions, *Geologiya i tektonika platform i orogennykh oblastei Severo-Vostoka Azii* (Geology and Tectonics of Platforms and Orogenic Regions of Northeastern Asia), Yakutsk: Geol. Inst. Sib. Otd. Ross. Akad. Nauk, 1999, pp. 52–61.